

Full length article

The resources, exergetic and environmental footprint of the silicon photovoltaic circular economy: Assessment and opportunities

N.J. Bartie ^{a,*}, Y.L. Cobos-Becerra ^b, M. Fröhling ^c, R. Schlatmann ^b, M.A. Reuter ^{a,d}^a Helmholtz-Zentrum Dresden-Rossendorf, Helmholtz Institute Freiberg for Resource Technology, Chemnitzer Straße 40, 09599 Freiberg, Germany^b Helmholtz Zentrum Berlin, PVcomb, Schwarzschildstr. 3, 12489 Berlin, Germany^c Professorship Circular Economy, Technical University of Munich, Am Esigberg 3/I, 94315 Straubing, Germany^d SMS Group, Eduard-Schloemann-Straße 4, 40237 Düsseldorf, Germany

ARTICLE INFO

ABSTRACT

Keywords:

Silicon photovoltaics
Circular Economy
Digital twin simulation
Neural networks
Exergy

The photovoltaic industry has shown vigorous growth over the last decade and will continue on its trajectory to reach terawatt-level deployment by 2022–2023 and an estimated 4.5 TW by 2050. Presently, its elaboration is driven primarily by cost reduction. Growth will, however, be fuelled by the consumption of various resources, bringing with it unavoidable losses and environmental, economic, and societal impacts. Additionally, strong deployment growth will be trailed by waste growth, which needs to be managed, to support Sustainable Development and Circular Economy (CE). A rigorous approach to quantifying the resource efficiency, circularity and sustainability of complex PV life cycles, and exploring opportunities for partially sustaining industry growth through the recovery of high-quality secondary resources is needed.

We create a high-detail digital twin of a Silicon PV life cycle using process simulation. The scalable, predictive simulation model accounts for the system's non-linearities by incorporating the physical and thermochemical principles that govern processes down to the unit operation level. Neural network-based surrogate functions are subsequently used to analyse the system's response to variations in end-of-life and kerf recycling in terms of primary resource and power consumption, PV power generation capacity, and CO₂ emission. Applying the second law of thermodynamics, opportunities for improving the sustainability of unit operations, the larger processes they are the building blocks of, and the system as a whole are pinpointed, and the technical limits of circularity highlighted. We show the significant effects changes in technology can have on the conclusions drawn from such analyses.

1. Introduction

Solar photovoltaics (PV) is one of the electricity generation technologies set to play a key role in the transition to low-carbon energy systems. Over the last decade, the global solar PV industry has grown at a rate of more than 35% annually, reaching record levels and outpacing annual conventional power capacity additions in many regions. At the end of 2019, the world's cumulative installed PV capacity was 583.5 GW with an annual module production capacity of 143 GW ([Fraunhofer ISE, 2020](#)). This exponential growth can be largely attributed to dramatic cost reductions ([VDMA, 2020](#)), solar technology innovation, and specific support policies aimed at reducing the price gap between PV and conventional electricity sources ([IEA PVPS, 2019](#)). The further development and deployment of solar PV can result in new business models that

stimulate industrial and employment growth ([Michas et al., 2019](#)). Industry forecasts project global installed PV power to reach the terawatt (TW) level by 2022–2023 ([Haegel et al., 2019](#)). The COVID-19 pandemic and associated market uncertainty and volatility has, however, exposed vulnerabilities such as the susceptibility of PV supply chains to shocks, and is highly likely to cause delays in several planned PV projects ([IEA, 2020a; NREL, 2020](#)). With a current share of 95% and its market dominance set to continue, crystalline Silicon (c-Si) PV is well positioned to increase the annual production of PV modules by 3–4 terawatts (TW) annually by 2040 ([VDMA, 2020](#)).

Several other costs, not just monetary but also in terms of resources, waste, and environmental, economic and societal impacts, are associated with industry growth. PV technologies rely on the availability of various materials, particularly Silicon metal in c-Si-based PV

* Corresponding author.

E-mail address: neill.bartie@gmail.com (N.J. Bartie).

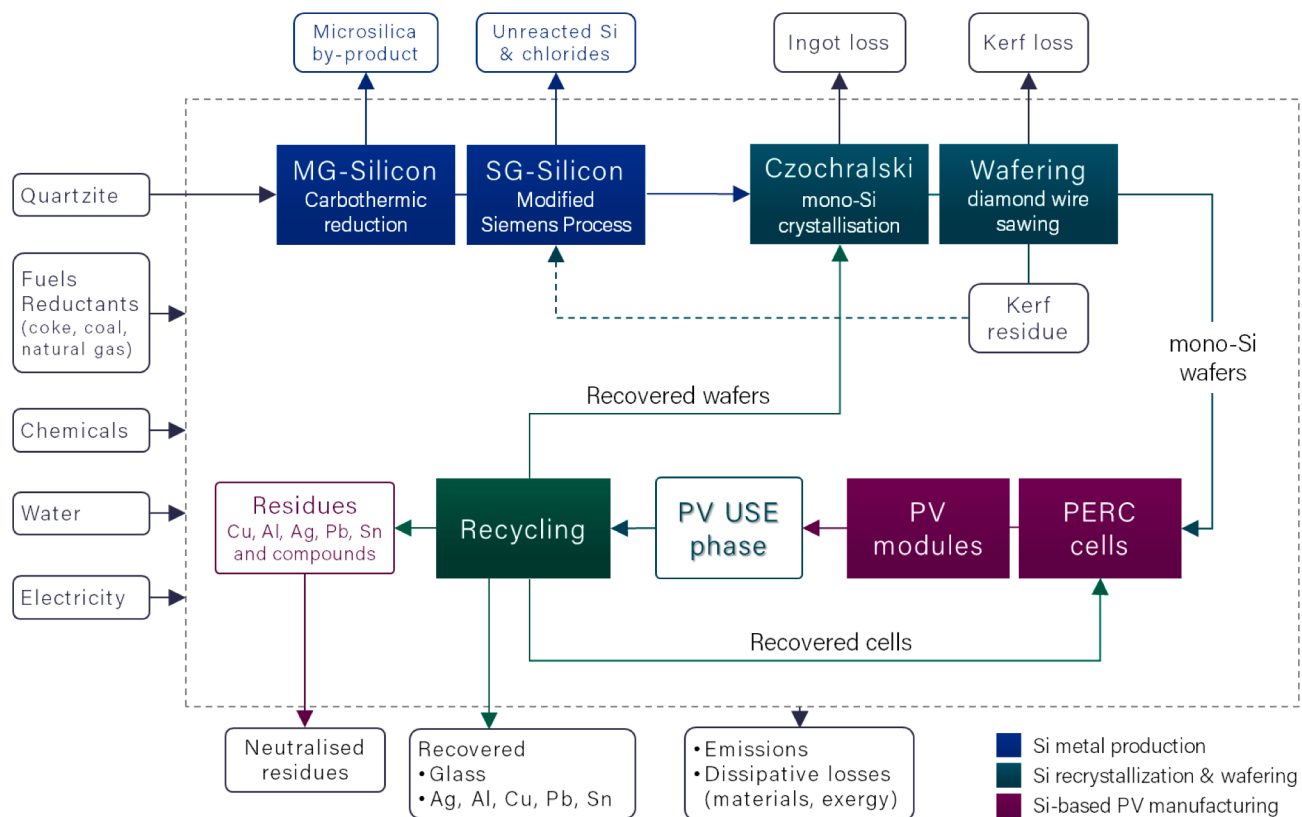


Fig. 1. mono-Si PERC PV life cycle system.

technologies, the high economic importance of which, together with its increased supply risk, justified its inclusion in the European critical raw materials (CRMs) list (European Union (EU), 2017a). Improvements in cell and module efficiencies and efforts to reduce material consumption have resulted in the amount of polysilicon needed per watt of power generated decreasing from 7.2 g/W in 2009 to 3.6 g/W in 2019 (Fraunhofer ISE, 2020; IEA PVPS, 2019). While this trend will cause a proportional decrease in Si demand, PV deployment will still cause a net increase—demand for the EU PV sector is expected to increase from 33 kt in 2015 to 235 kt in 2030 (European Commission, 2018). Furthermore, end-of-life (EOL) PV module quantities are expected to increase significantly between 2020 and 2030 because of modules commissioned over the last few decades now beginning to come out of service—the global waste-to-new installation ratio is expected to increase from 4 to 14% in 2030 to over 80% by 2050 (Sica et al., 2018). With cumulative global PV waste quantities forecast to reach 8 million tonnes by 2030 and ten times as much by 2050 (Heath et al., 2020), the need for increased focus on design-for-X (DfX, where X refers to e.g. circularity, sustainability, disassembly, or recycling), and for actions that foster the development of circular business models and sophisticated recycling processes capable of recovering high-purity Si and other materials, is clear.

It should be noted that projections of waste quantities are based on the assumption that PV modules reach EOL once their power generation efficiency has deteriorated to about 80% of the nameplate efficiency. This technical lifetime is typically 25 to 30 years; it does not mean that modules are no longer useful after this period. However, several factors come into play considering the trade-offs between recycling and re-use after the first lifetime. For utility-scale installations, Wade et al. (2017) found that high-value recycling provides an economic incentive as the revenue from recycled materials would exceed decommissioning costs. Furthermore, the probability of the levelized cost of electricity (LCOE) from a re-use system being lower than that from a new system at the same location is less than 10% (Wade et al., 2017). Aside from purely

economic considerations, the export of modules for re-use to e.g. first world or developing countries risks, inter alia, the informal recycling of second-life EOL modules at standards below those prescribed by European health and safety regulations, potentially creating negative environmental and social impacts in communities already at a disadvantage relative to European living standards. On the other hand, such exports could provide these communities with access to electricity for the first time. Re-use also lowers environmental impact by increasing life cycle power generation without the additional materials and energy consumption associated with manufacturing (Heath et al., 2020). As stated by Tsanakas et al. (2020), research to date have been somewhat biased towards recycling, leaving many of these trade-offs as yet unexplored. Ongoing projects like CIRCUSOL (circusol.eu) aim to formalize PV industry value chains for repair, refurbishment and re-use, and to develop more circular PV business models (Tsanakas et al., 2020).

While recycling aims to close material loops to maximise resource efficiency (RE), the seldom-discussed quandary is that no such loop can be closed entirely—any real transformation process is always subject to material and energy losses because of inevitable inefficiencies and the creation of entropy. Therefore, the identification and minimisation of these along entire life cycles, not just at EOL, are key (Reuter et al., 2019). If not accounted for, losses cannot be ‘designed out’ because the need for innovation would not be identified in the first place. All of these effects, as well as environmental, economic and social impacts need to be quantified in the conceptual and early design phases, so that efforts typically focussed on PV-specific cost reductions and power conversion efficiency (PCE) improvements can be evaluated within the bigger picture of entire product life cycles, sustainability and CE. Without such comprehensive assessments, the true contribution of the PV industry to decarbonisation and achieving sustainable CE would be difficult to ascertain.

This paper provides insights on the resource and sustainability performance of the mono-Si PV module life cycle using the PERC cell architecture. We apply the methodology presented in a previous

Table 1
Cases mapped on the parameter space.

	Base case	Case 1	Case 2
Primary mineral resource			
Quartzite	Fixed*	Fixed*	Fixed*
Secondary resources			
EOL modules	Not recycled	95% recycled (as SG-Si)	95% recycled (as SG-Si)
Kerf residues	Not recycled	Not recycled	50% recycled (as MG-Si)

* Fixed at various levels, as specified in the text and in Figures.

publication, in which the resource consumption (RC), RE, and environmental impacts of the cadmium telluride (CdTe) PV module life cycle were assessed (Bartie et al., 2020), to create a similar digital twin for the c-Si PV life cycle. Detailed, highly disaggregated digital twins enable the quantification of resource requirements as well as potential sustainability impacts using up-to-date equipment and operational information, for both current technologies and those under development. In doing so, there is the potential to facilitate DfX by complementing design activities with resource and sustainability information. The simulation-based approach takes into consideration the many non-linear physical, chemical, and thermodynamic transformations that govern production and recycling processes, as opposed to somewhat oversimplifying approaches that sometimes apply outdated process data to current and developing technologies. Comprehensive inventory databases, albeit extremely useful sources of information, do not yet include data for e.g. mono-Si PERC cells and other newer technologies; a significant proportion of source data for Si-based modules date back to between 2011 and 2015 (e.g. Frischknecht et al., 2020). The application of older data to newer technologies, and the use of linear, mass-based material flow analyses, could lead to inaccuracies as well as the exclusion of thermodynamic processes and non-linearities from assessments, especially where recycling loops are present. For this paper, we exclude the use phase as it has virtually no emissions (Muteti et al., 2020), and the impacts of material transfers between life cycle steps as it is assumed that all value chain stakeholders are co-located. The focus is on the effects of recycling on the resource efficiency and carbon footprint of the system. The scenarios investigated, and the methods used are described in Section 2, and results are presented and discussed in Section 3. The paper is concluded and future work briefly discussed in Sections 4 and 5, respectively.

2. Methods

2.1. System and scenario definition

The life cycle system analysed in this paper is shown in Fig. 1 and consists of the following processes:

- 1 Metallurgical grade silicon (MG-Si) production through carbothermic reduction of silica (SiO_2) with ladle refining,
- 2 Solar grade silicon (SG-Si) production using the Siemens process,
- 3 Monocrystalline silicon (mono-Si) ingot crystallisation via the Czochralski (Cz) process, wafer cutting using diamond wire sawing (hereafter also referred to as *wafering*), and the recycling of kerf residue,
- 4 Production of PV cells of the PERC design,
- 5 PV module assembly, and
- 6 EOL recycling, consisting of thermal delamination and polymer combustion, followed by leaching/etching processes that aim to recover valuable and hazardous metals/compounds.

We cover the parameter space that includes the full ranges of EOL and kerf (a residue that forms during wafering) recycling rates, and map the cases shown in Table 1 onto this space. The base case, a linear

production scenario in which no recycling takes place, serves as a reference. In Case 1, 95% of the produced PV modules are collected and all enter the EOL recycling process, while all kerf residue is lost. Case 2 builds on Case 1 by additionally recycling of 50% of the kerf residue. The Si recovered from EOL modules is recycled to the Cz process at SG-Si grade, while kerf residue is recycled to the Siemens process at MG-Si quality. The recycling of kerf residue at SG-Si quality is briefly explored (not shown in Fig. 1).

For comparison, the solution space for a scenario that represents a complete process change—replacing the Siemens process with a silane (SiH_4) fluidised bed reactor (FBR), and changing from mono-Si to multicrystalline silicon (mc-Si)—is presented in Section 3.4.

The methods employed are described in Section 2.2. Descriptions of the production and recycling processes and assumptions can be found in the Appendix.

2.2. Methods used

2.2.1. Process simulation

Understanding the mass and energy flows through production systems is essential for their design, simulation and optimisation, and to manage their complexity and interconnectedness (Fröhling et al., 2013; Klatt and Marquardt, 2009; Reuter, 1998, 2016). The laws of conservation dictate that mass and energy must balance over every piece of equipment, process chain and system, and the second law of thermodynamics (SLT) states that any real process can only occur in the direction of increasing entropy. At its core, process simulation (PS) is based on these principles—incorporating large databases of the physical, chemical and thermodynamic properties of tens of thousands of metals, minerals and other compounds, PS platforms enable detailed analysis, complying with the laws of conservation and the SLT at every step. Therefore, these constraints are implicit and ensure that the laws of physics are not violated (Diwekar and Small, 2002). Instead of assuming linearity over large process blocks, processes are disaggregated into their constituent unit operations and relevant thermochemical and physical transformation processes used to determine input-output relationships over each unit. The distribution of valuable and hazardous substances are calculated and predicted where they occur, making it possible to allocate emissions to the correct outputs, to identify consumption and pollution hotspots, to maximise recovery of materials and energy, and to minimise entropy creation. This is the minimum level of detail required to characterise process and recyclate flows, the extent of downcycling, and processes' contribution to sustainable development and CE (UNEP, 2013). Representative simulations rely on high-quality input data and in-depth knowledge of metallurgical and other processing options and their limits (Verhoef et al., 2004; Reuter, 1998, 2016), which requires industry buy-in and collaboration.

Applying the above principles, the HSC Chemistry platform, HSC Sim (Outotec, 2020) is used to create a high-resolution digital twin of the mono-Si PV life cycle system to assess its resource and environmental performance. For each process block shown in Fig. 1, the constituent unit operations are separately modelled and connected to create a simulation for that process. The processes are then connected to create a closed-loop industrial symbiosis system that represents the life cycle. The effects of solution chemistry and entropy creation are accounted for by means of Gibbs free energy minimisation in HSC Chemistry and FactSage (version 7.2) (GTT-Technologies, 2020), as well as phase diagrams, Pourbaix (E_h -pH) diagrams for aqueous solutions, and Ellingham diagrams to estimate product compositions and process requirements. The result is a deterministic simulation model of the entire life cycle, in this case comprising 75 unit operations, 334 streams and 163 species. It is parameterised by various physical relationships, chemical reactions, thermodynamics, and constants, and validated against known operating points and industrial reality. Using such a model, blanket assumptions of linearity for complex processes and systems are largely avoided. The simulation is used to predict the system's response to changes in the

input variables—in this case EOL and kerf recycling rates at constant quartzite consumption—over the ranges defined in Table 1.

2.2.2. Exergy analysis

As mentioned, the SLT states that entropy must increase for any real-world process to take place. Exergy, which represents the *quality* of an energy quantity, is dissipated as entropy increases. Therefore, all real transformation processes occur with an unavoidable level of inefficiency. Contrary to mass and energy, therefore, exergy is not conserved and does not balance over real processes—the exergy dissipated i.e. the *imbalance* is referred to as the irreversibility of the process at hand. Dissipated exergy can only be restored through input from outside of the system (Dincer and Cengel, 2001), which, in turn, cannot happen without exergy dissipation in another system. In other words, we are caught in a spiral of ever-decreasing exergy as the system gradually approaches equilibrium with its surroundings. Complete equilibrium is not a desired outcome if products are to be kept in circulation for as long as possible—the dissipation of exergy should be counteracted or prevented from happening in the first place. Manifestations of the law can be observed, for example, when metals or other compounds are intentionally or unintentionally combined or dissolved into one another, at the outset likely to endow products with specific functionalities, but ultimately to the detriment of EOL treatment efficiency and recyclate purity. As compounds are exposed to contaminants during recycling, entropy increases further, again causing decreases in quality (Amini et al., 2007). This downcycling can only be countered by valorisation processes that themselves dissipate exergy. The material and energy resources required for these can only come into being if exergy is dissipated elsewhere. This highlights the critical importance of DfX in the early stages of sustainable production and supply chain design.

Exergy analysis provides a useful set of tools with which to keep track of the locations and magnitudes of these degradations, for material and energy simultaneously, highlighting opportunities for improvement. We use the *exergy efficiency* of processes and systems, and the *exergy cost* (Lozano and Valero, 1993) for intermediate and finished products as proxies for RE and RC, respectively. More detailed explanations of calculation methods can be found in previous publications (Bartie et al., 2020; Abadías Llamas et al., 2019).

2.2.3. Neural networks

For complex, non-linear life cycle simulations such as that presented in this paper, computational time and intensity can become problematic. Neural networks (NN) can be used to model input-output interrelationships in highly complex systems (Casalino et al., 2016), allowing for generalized non-linear process modelling without the need to predefine regression equations (Reuter et al., 1992). NNs are, therefore, useful tools with which to create surrogate functions for the input-output relationships of interest while considering the entire system's response. Aiming to emulate how neurons in the brain fire to transmit information, NNs consist of layers of neurons. Each neuron is a computational unit that transforms a weighted sum of its inputs into an output using an activation function, for which the non-linear sigmoid function is typically used (Kubat, 2017). The weights are the NN's degrees-of-freedom, the number of which depends on the number of neurons used. The NN learns via a training function that adjusts the weight of each input into each node iteratively until the overall input-output error is minimised. We implement a basic NN architecture, a multilayer perceptron, to emulate process simulation results.

The first step in creating a NN is to generate the dataset needed to train, validate, and test it. To this end, HSC's scenario editor is used as follows:

- Random combinations of the three independent variables (quartzite consumption, and EOL and kerf recycling rates) are generated by randomly sampling from a continuous uniform distribution over specified data ranges.

- The simulation is run with each set of inputs to calculate the system response. Here, each run requires 21 iterations to converge.
- Thirty-two dependant variables are read from the simulation into the dataset and a further 40 calculated.
- For the results presented in this paper, the exercise was repeated 3070 times i.e. performing 63,170 simulation iterations.

MATLAB's (MathWorks, 2020) NN user interface (*nntool*) is used to generate the code that initiates, trains, tests and validates the networks. The dataset is imported and randomly divided into three subsets such that 70% of the 3070 data combinations is used for network training, 15% for testing, and 15% for validation. During network training, the validation error decreases but could increase again if over-training occurs, the equivalent of the NN 'memorising' the dataset instead of learning to generalise. Using the MATLAB tool, network training stops once a validation error increase is detected over six consecutive iterations (MathWorks, 2020c). We use small, shallow perceptrons comprising three neuron layers to minimize the number of weights without restricting the NN's ability to learn the input-output relationships effectively (Reuter et al., 1992). A schematic representation of such a network and its relation to the process simulation is shown in Fig. A1.1.

A separate single-output NN (such as that shown in Fig. A1.1) is created for each dependant variable of interest. For the results presented in this paper, these include power consumption and CO₂ emissions during production and recycling, and nominal PV power generated. All these NNs have the same inputs i.e. the amount of quartz consumed for Si production, the module EOL recycling rate, and the kerf recycling rate. The number of hidden neurons is kept to a minimum to ensure that the ratio of samples to degrees-of-freedom is high, and is chosen as the smallest number that produces a stable NN i.e. one that produces the same result every time it is called. Stability is evaluated visually by running the NN repeatedly, and by comparing regression coefficients and validation errors obtained for different numbers of hidden neurons. We generally obtain the best results with a hidden layer width of three to four neurons using the *Bayesian regularization backpropagation* training function (*trainbr*), which "updates the weight and bias values according to Levenberg-Marquardt optimization" and "minimizes a combination of squared errors and weights, and then determines the correct combination so as to produce a network that generalizes well" (MathWorks, 2020b). In this case, redundancies vary between 146 and 192. This approach reduces the risk of overtraining a NN to the quirks of the specific dataset used for its training.

2.2.4. Environmental impact

Carbon footprints are evaluated for the cases in Table 1, focussing on direct (Scope 1) and electricity-related (Scope 2) emissions (Greenhouse Gas Protocol, 2011). To ensure consistency and compliance with the laws of physics, the system boundary is exactly that of the process simulation. In processes with multiple outputs, overall environmental impacts need to be distributed between products sensibly. We largely avoid allocation by disaggregating the life cycle into individual unit processes (Ekval and Finnveden, 2001), allowing for actual emissions to be quantified where they are generated.

The simulation-based approach expands the foreground system, so avoiding the over-use of aggregated databases to populate background system inventory. It also allows for individual process steps and production routes to be optimised or updated to reflect current technologies and up-to-date operating parameters, and for emissions data to be updated accordingly. Furthermore, it allows for reactors and equipment, production routes and supply chains (potentially regionally distributed) to be configured for the study at hand. The databases remain valuable and essential tools, however.

CO₂-equivalent direct emissions (Scope 1) are obtained from chemical reactions defined for individual process steps in the process simulation. Scope 2 emissions are determined from the power requirements

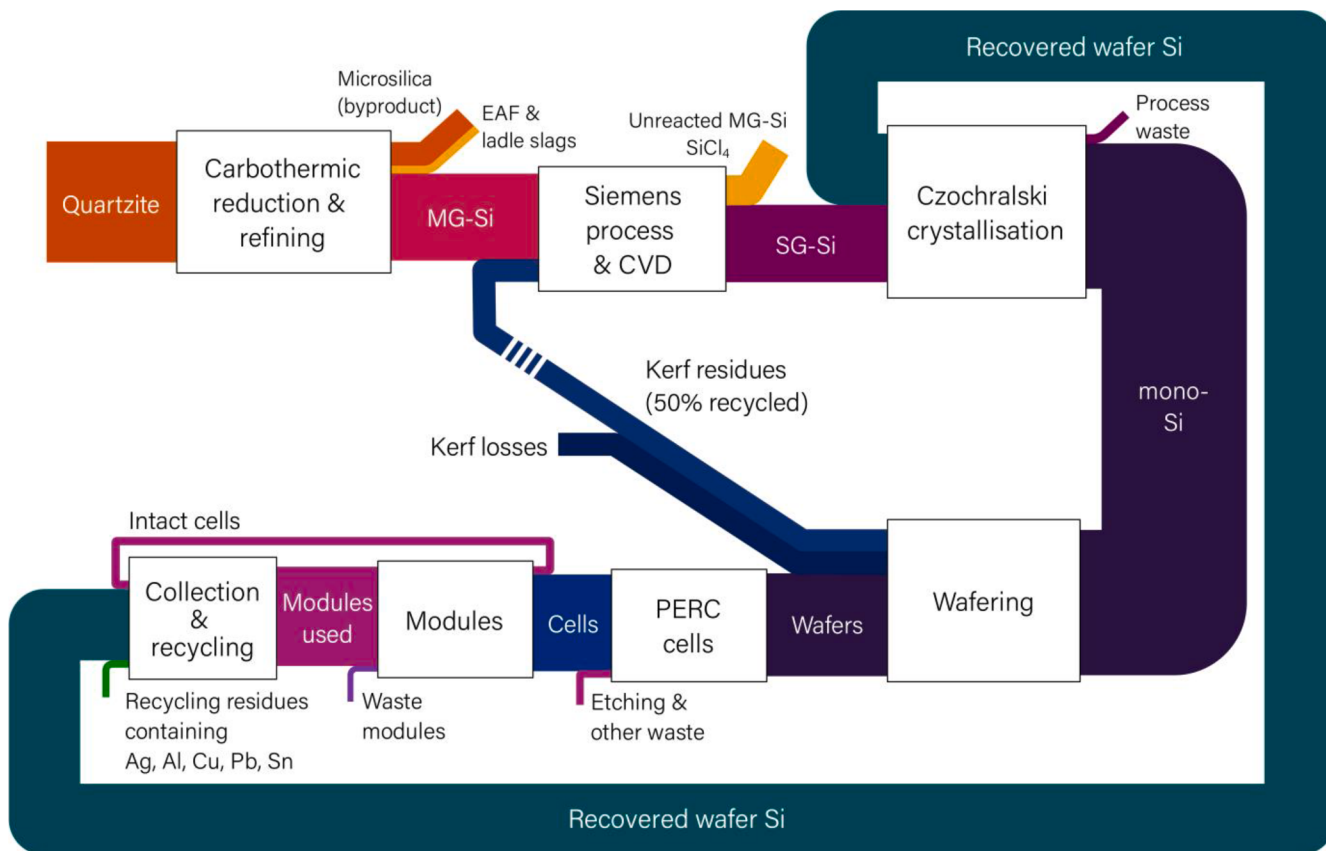


Fig. 2. Silicon balance for the life cycle with 95% EOL recycling and 50% kerf recycling (SiO_2 in glass excluded).

determined in the simulation and the emission factors for regional energy grid mixes from the GaBi database (thinkstep, 2018). Background process emissions (Scope 3) are only included for PV module glass, aluminium frames, mounting systems and cabling (De Wild-Scholten, 2013; Frischknecht et al., 2016; Stoltz et al., 2017). Because of excluding other background emissions and simulating a closed-loop system, absolute CO₂-equivalent emissions presented here cannot be compared with other studies directly. As mentioned, we exclude the use phase as its emissions are virtually negligible, and the impacts of material transfers between life cycle steps, as it is assumed that all stakeholders are co-located.

3. Results and discussion

In this section, findings are reported for two key aspects of the life cycle: *material and energy resources* (consumption and efficiency) and *environmental impact* (in terms of CO₂ emission).

3.1. Conservation law analysis (based on balanced mass and energy flows)

The laws of conservation state that mass and energy must balance over all processes. The steady-state Si mass balance shown in Fig. 2 clearly shows the locations and relative magnitudes of Si-containing streams in the life cycle for Cases 1 and 2. Note that line thicknesses are to scale for total Si mass flow.

The *Recovered wafer Si* loop results from the 95% EOL recycling. Total kerf residue is shown as the two diagonal streams exiting wafering. With the progress already made, and with ongoing kerf recycling R&D, the assumption of 50% kerf recycling as MG-Si is believed to be conservative in terms of both quantity and quality. Based on the

parameterisation of our simulation, considerable amounts of Si also leave the system as microsilica from MG-Si production and as unreacted MG-Si and SiCl₄ from the Siemens process.

3.1.1. Effects of recycling on nominal PV power production

As an example in the base case, 100 kt of quartzite consumption allows for a nominal PV power production of 10.4 GW_{peak}. In Case 1, this value increases by 86% (to 19.4 GW_{peak}) without additional quartzite consumption, and in Case 2 by 136% (to 24.5 GW_{peak}), the latter greater than 100% because, in this simulation, quartzite consumption is not displaced by the recycled Si. Without kerf recycling, primary quartzite consumption would have to increase to 126 kt to produce the same amount of modules, and to 237 kt if no recycling took place at all.

The combined effects of EOL and kerf recycling at fixed levels of quartzite consumption is shown in Fig. 3. Response surfaces show that the effect of EOL recycling on PV power production is non-linear, and that kerf recycling amplifies the benefits of EOL recycling i.e. the module production increase is stronger when kerf recycling complements EOL recycling. The three scenarios mentioned above are indicated as points on the response surface. Note that the non-linearity cannot be attributed to a single factor—it is rather a result of the recycling loops and various non-linear relationships that define the simulation.

Two additional data points are shown to put these numbers into perspective. In 2019, 4 GW_p's worth of PV modules were installed in Germany (Fraunhofer ISE, 2020), which, in our Case 1 simulation equates to a primary quartzite consumption of 20.5 kt. Without recycling, 38.6 kt of quartzite would be needed. Similarly, the EU-28's 16.7 GW_p (Fraunhofer ISE, 2020) corresponds to the consumption of 85.5 kt quartzite with 95% EOL recycling and 161.0 kt without recycling. Fig. 3 quantifies the potential benefits of EOL, kerf and combined recycling at the RC/PV-power nexus, and highlights how system circularity can be

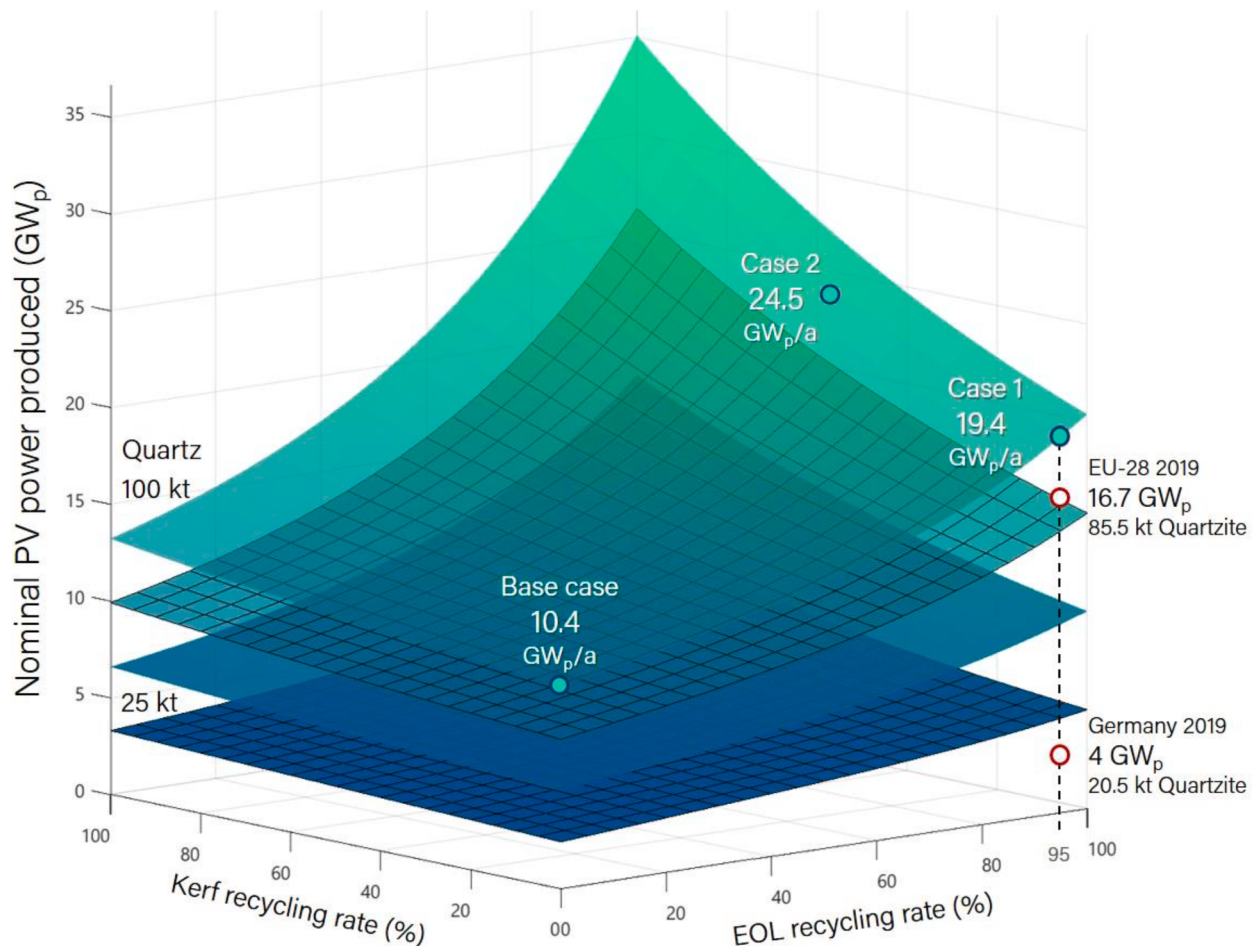


Fig. 3. The combined effects of EOL and kerf recycling on nominal PV power production at a nominal area efficiency of $230 \text{ W}_{\text{p}}/\text{m}^2$ (surfaces of constant quartz consumption are shown for reference).

used as a tool to help sustain projected PV deployment growth.

3.1.2. Effects of recycling on power consumption

Combining the above with a similar analysis of power consumption reveals the effects of recycling on power consumption per module area produced. Fig. 4 shows that EOL recycling reduces power consumption significantly, from $116 \text{ kWh}/\text{m}^2$ without recycling to $75 \text{ kWh}/\text{m}^2$ for Case 1, a 35% reduction. This can be explained by the fact that EOL-recycled Si bypasses both MG-Si production and the Siemens process, the largest electricity consumer in the system. The additional benefit of kerf recycling is small ($73 \text{ kWh}/\text{m}^2$ compared to $75 \text{ kWh}/\text{m}^2$ for Case 1) because of kerf still going through the Siemens process (see Fig. 2). If future treatment processes were to recover kerf at SG-Si quality, energy savings would self-evidently increase. For Case 2, the simulation predicts a consumption of $64 \text{ kWh}/\text{m}^2$ when kerf is recycled into the Cz process instead—a 45% decrease from the base case. This excludes the energy consumption of any potential kerf treatment process, however, and may be overoptimistic.

3.1.3. Material efficiency of the recycling process

The recycling process (described in the Appendix) claims to recover 74% Ag and 83% Cu, and 85–90% wafer Si at SG-Si quality, and can remove at least 99% of Pb^{2+} from solution (Huang et al., 2017). Applying these recoveries to the EOL-recycled modules and assuming a 5% loss of wafers and strings during the dismantling and combustion steps, the overall metal recoveries shown in Fig. 5 are achieved.

Module composition and potential metal and other material recoveries are given in Table 2.

With an average Ag price of \$521.48/kg in 2019 (macrotrends.net), potential revenue is approximately \$109/tonne recycled (\$2.60/module). Similarly, with the average Cu price of \$7.29/kg, potential revenue amounts to \$55/tonne recycled (\$1.31/module) excluding cables, assuming that metals are recovered at saleable purity. This translates to an estimated revenue of \$8.2 million per nominal GW_{p} for Ag and Cu alone. This is a rough indication based on present-day technology and economic conditions, however, as PV module lifetime, the cost of recycling, and technological developments such as the decreasing trends in Ag and Cu consumption (VDMA, 2020), amongst others, have not been considered in this paper.

3.2. Exergy analysis (application of the SLT)

3.2.1. Exergy dissipation and efficiency

As mentioned, exergy efficiency and cost are used as proxies for RE and RC, respectively, thus taking a thermodynamic perspective. Fig. 6 shows the relative magnitudes of exergy flows through the system for Case 2. Stream colours are designated as follows:

Dark blue: material and energy inputs from outside of the system (from the technosphere),

Yellow: waste streams and emissions (to the environment),

Green: byproducts and potentially useful streams to be treated outside of the system (to the technosphere),

Light blue: internal transfers of products,

Brown: internal recycle streams,

Orange: dissipated exergy i.e. the amount needed to close the exergy balance, representing the losses resulting from the creation of entropy.

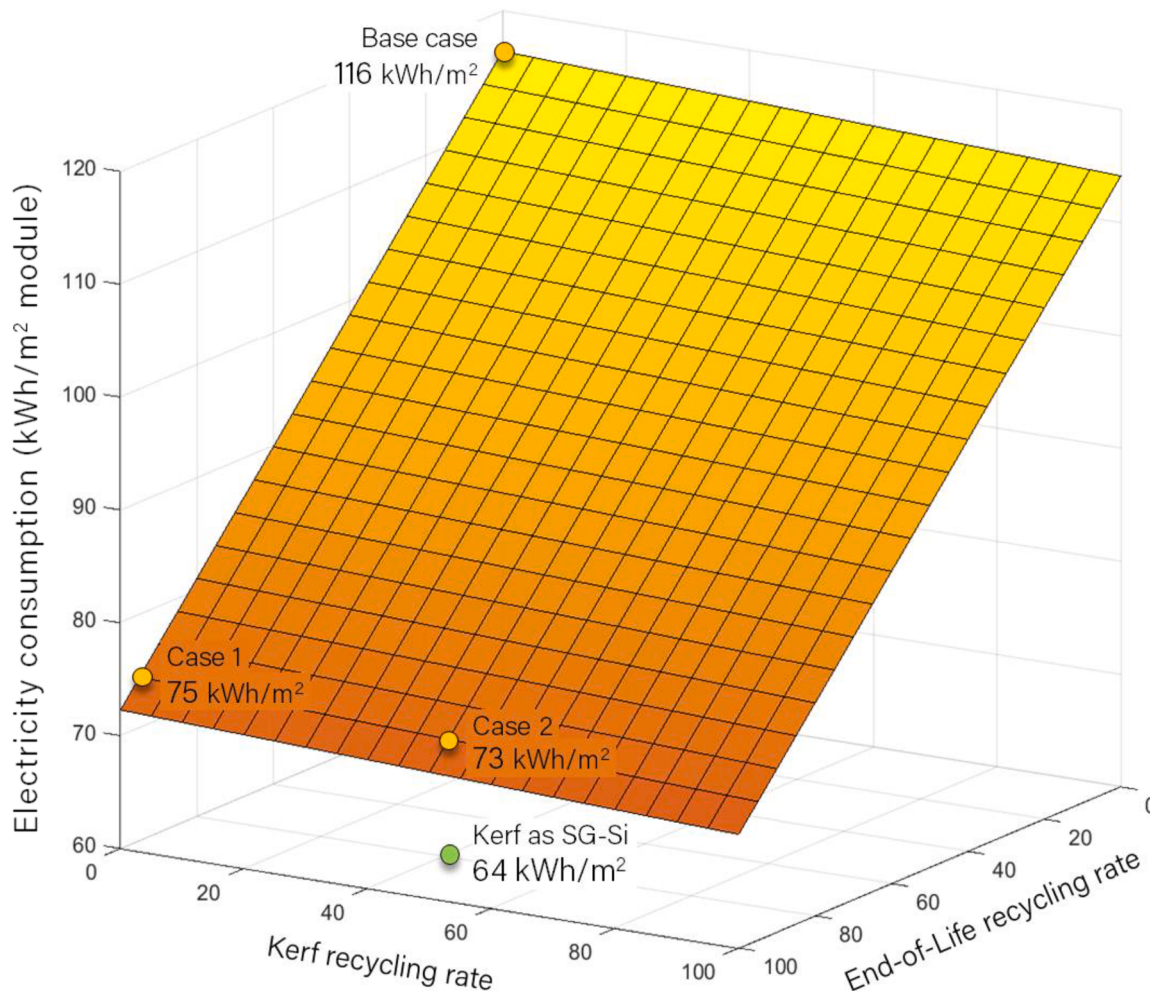


Fig. 4. Variation of specific power consumption with EOL and kerf recycling rate (axis directions are opposite to those in Fig. 3 for the sake of readability).

From Fig. 6, it is clear that the SG-Si and Cz processes consume large amounts of exergy (dark blue) relative to the intended onward exergy flows (light blue). These processes, followed by recycling and cell manufacturing, also dissipate the most exergy (orange). Module production, on the other hand, consumes a sizeable amount of exergy but does so efficiently with relatively little exergy dissipation (orange).

Associated exergy efficiencies are shown in Fig. 7. Also shown are efficiencies for a hypothetical zero-waste scenario in which all material and energy losses (yellow) are considered to be resources i.e. all waste have been “designed out” as promoted by prominent CE organizations. The difference between the two efficiencies represents, therefore, the theoretical RE improvement potential if it were possible to eliminate or transform all losses into resources. This should be what is aimed for in all the DfX domains. Highlighting the two process steps with the largest differences between the two efficiencies, and therefore opportunities for waste reduction: in the Cz and wafering processes, the difference is attributed to water treatment residues and the 50% kerf loss. In the PERC cells process it is the result of losses from the layer deposition steps and the wafer texturing liquor.

Important to note is that even zero-waste efficiencies are well below 100%, the primary cause being the inevitable dissipation of exergy. Thus, even if material loops could be closed, total circularity is impossible when exergy dissipation is accounted for. Fig. 7 is, therefore, a representation of the thermodynamic *limits of circularity*. However, by minimising exergy dissipation through optimisation and innovation in technology, processes and supply chains, the root causes of open loops e.g. downcycling, carbon emission and energy loss will be addressed

automatically as these are the main dissipaters of exergy. Waste heat recovery and reducing the consumption of electricity and high-carbon feed materials like fossil fuels, polymers and other organic compounds are good starting points, as these carry significant amounts of exergy that are usually dissipated in their transformation processes. In this paper, the maximum efficiencies represent our simulation model in its current configuration only, and cannot be applied to other systems.

3.2.2. Exergy cost

Analogous to monetary cost, exergy cost is an accounting quantity that represents the thermodynamic cost of a product, based on the theory of exergetic cost (Lozano and Valero, 1993). While exergy itself is not subject to the conservation laws, exergy cost is additive i.e. the exergy cost of a product is the sum of the costs of its constituents. It allows for the specific causes of exergy dissipation and their relative contributions to be identified, as is shown in Fig. 8. For the production of PV modules, our simulation gives an exergy cost of 50.3 kWh/m² (or 98.8 kWh/module). Note that, while exergy cost is expressed in kWh, it represents exergy dissipation from both energy and material streams. For comparison, we found the specific exergy cost for CdTe PV to be 118 kWh/module (Bartie et al., 2020).

The largest contributor to module exergy cost is the Cz process (31%), followed by deposition of the AlO_x cell layer (14.5%), phosphorous deposition (9.6%), wafer sawing (8.4%), and SiN_x deposition (8.4%). Based on our simulation, innovation in these processes would realise the greatest decreases in RC. In the Cz process, irreversibility mainly stems from power consumption and the subsequent loss of waste

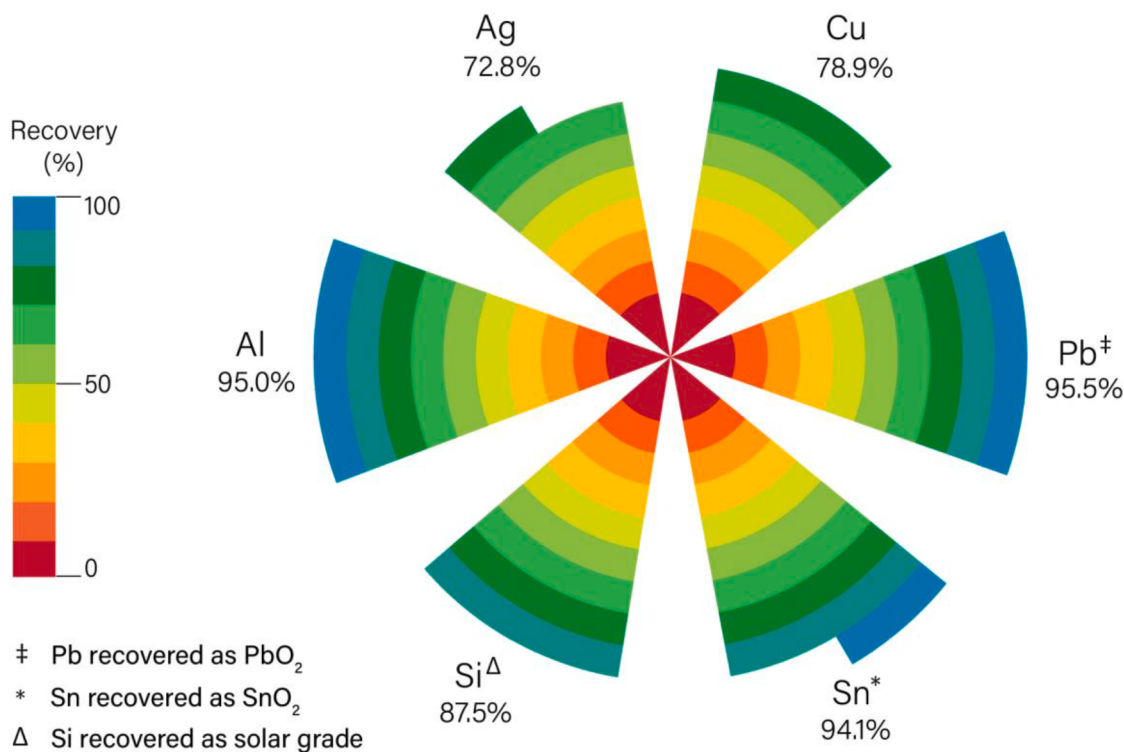


Fig. 5. Metal recoveries from the simulated recycling process.

Table 2
Module composition and material recovery.

Component	Content (kg/t module)	Recovered [†] (kg/t module)
Al (as Al ₂ O ₃ , excl. frame)	2.728	2.332
Ag	0.3313	0.2096
Cu	10.86	7.532
Pb (as PbO ₂)	0.07797	0.06703
SnO ₂	6.045	5.111
Si (solar grade)	30.98	24.15
Glass	661.0	654.4*
Polymers	111.3	–
Rest	1.243	–

† excluding intact cells (10% assumed in this paper).

* based on an estimated 99% glass recovery (Heath et al., 2020).

heat. This is also the case for the deposition and wafering processes, with smaller amounts of dissipation resulting from material losses. The rest contribution (13.5%) consists of those for the Siemens CVD reactor; module soldering, edge sealing and framing, and several others, each with an impact of less than 1%.

3.3. Carbon emissions

Total CO₂ generation is determined as the sum of (i) that generated directly in each process step (described in Section 2.2.4), (ii) 1.1 kgCO₂/kg glass (thinkstep, 2018), (iii) 62.4 kgCO₂/m² for the frame, mountings, cables, and connectors (Wernet et al., 2016; De Wild-Scholten 2013), and (iv) that associated with the electricity/fuel consumption of individual process steps. Fig. 9 shows the CO₂-equivalent emission per module area produced for the German energy grid mix and quantifies the sustainability increases potentially achievable via increased circularity. For the base case, emissions amount to 146 kgCO₂/m², decreasing by 14% (to 125 kgCO₂/m²) for Case 1 and by 15% (to 124 kgCO₂/m²) for Case 2. As for power consumption (Fig. 4), the decreases can be attributed to EOL recycling bypassing the Siemens process, while kerf

recycling does not. Similarly, the upgrading of kerf residue to SG-Si purity before recycling could bring about further decreases in CO₂ emission, in this case a further 3% to 120 kgCO₂/m². It highlights and quantifies the potential benefits of innovation in kerf recycling, so as to upcycle it to higher value solar grade purity, in which case it would also bypass the Siemens process.

While direct CO₂ emissions remain constant for a given production configuration, total emissions depend strongly on the energy grid mixes at production locations. Fig. 10 depicts the same information as Fig. 9 for the energy grids of various other countries, assuming that all life cycle steps are co-located.

With the high proportion of hydroelectricity, Norway is clearly the best performer with the lowest absolute emissions. Interestingly, because process-generated (Scope 1) emissions comprise almost 88% of the total (Scope 1 + 2) on the Norwegian grid, the benefit of bypassing the Siemens process is outweighed by process-generated CO₂—EOL recycling increases net emissions slightly, hence the reversed slope for the Norway surface. For the other regions, the Scope 1 share ranges between 18 and 42%, making the effects of changes in grid-related emissions more pronounced. Australia's and China's high reliance on coal make them the worst performers. In a hypothetical situation where the entire system is located in either Norway or Australia, CO₂ emissions are a factor of 2.3 higher in Australia with no recycling, and 1.8 times higher for Case 2 because of the dominance of fossil fuels in the grid mix, as is also the case for China. Europe's Si metal imports originate primarily from Norway and Brazil, the two best performers, and to a lesser extent from China (European Union (EU), 2017b). At present, only China holds the full supply chain domestically.

3.4. Technology change

A total technology change can affect the system significantly in terms of RC and impacts. Fig. 11 depicts normalised response surfaces for absolute power consumption and CO₂ emission for the current system and shows that they trend in the same direction. Increased recycling leads to more modules being produced, higher CO₂ generation during

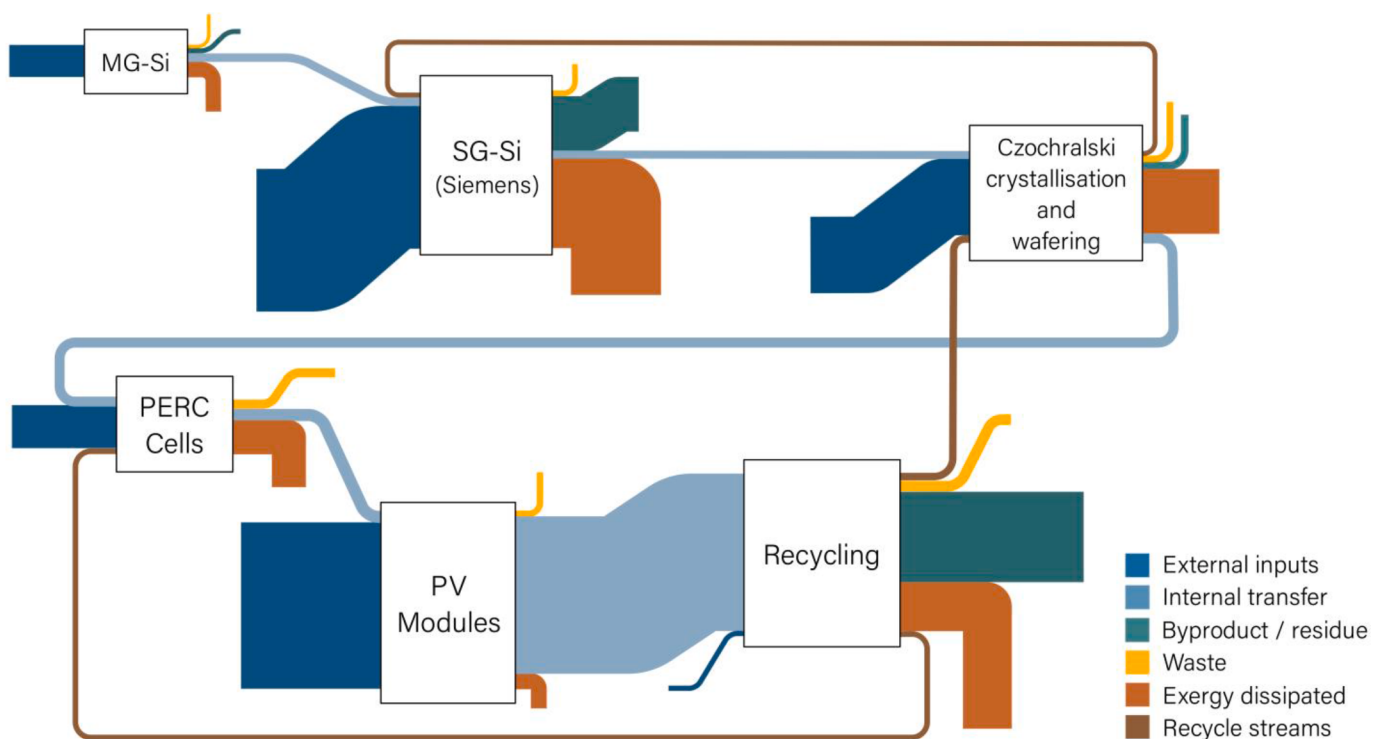


Fig. 6. Flows of exergy through the mono-Si life cycle (Case 2).

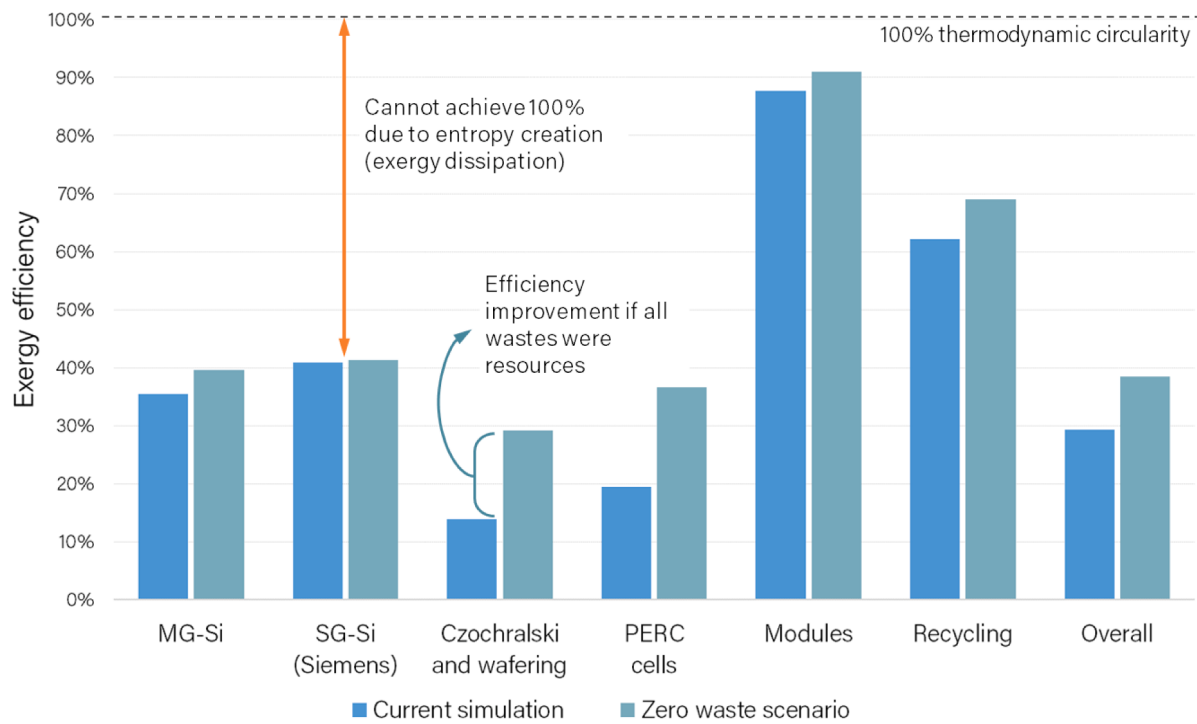


Fig. 7. Exergy efficiency for each process in the life cycle based on Case 2 and for a zero-waste scenario (note that overall efficiency is not the product of individual efficiencies, as each process step has external inputs).

polymer incineration, and higher net power consumption.

Fig. 12 shows the equivalent surfaces for a system in which SG-Si is produced via the silane FBR route, and mc-Si is used instead of mono-Si.

Here, surface slopes are *opposite* with respect to EOL recycling. As EOL recycling increases, net CO₂ emission increases due to increased polymer incineration. At the same time, the additional power generated

via heat recovery decreases the net power requirement. In contrast, the Siemens process completely absorbs the power generated from waste heat in the mono-Si system. This highlights the importance of waste heat recovery in balancing overall system power consumption. To further illustrate potential differences, Fig. 13 shows that, on average, CO₂ emission per module area for the FBR process is around 27% lower than

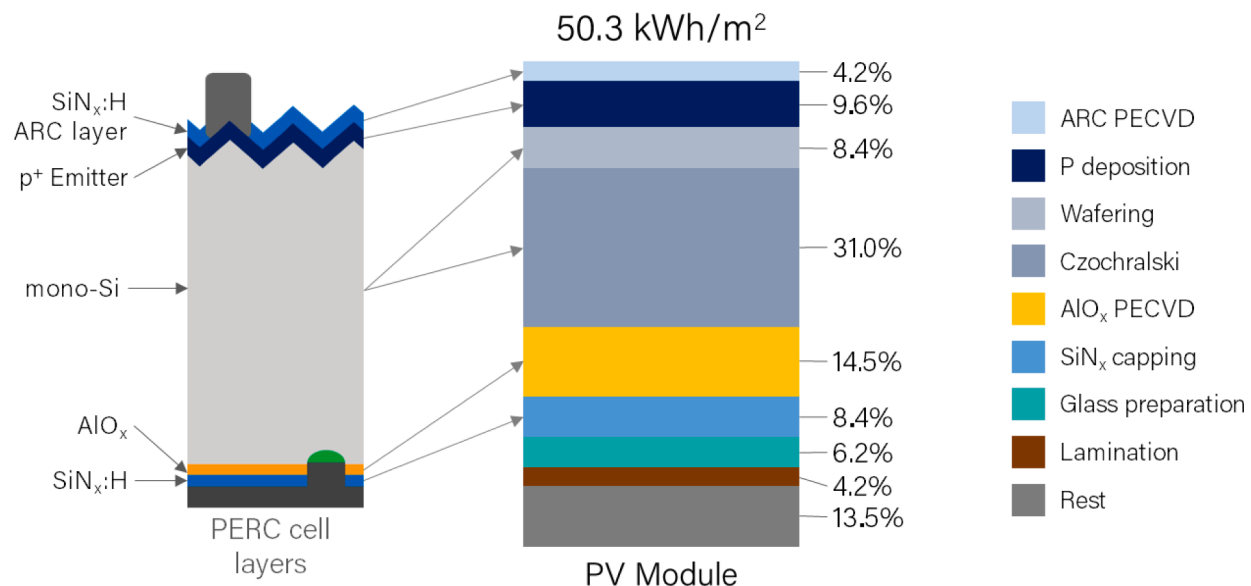


Fig. 8. Breakdown of contributions to overall module exergy cost (links to PERC cell layers shown on the left).

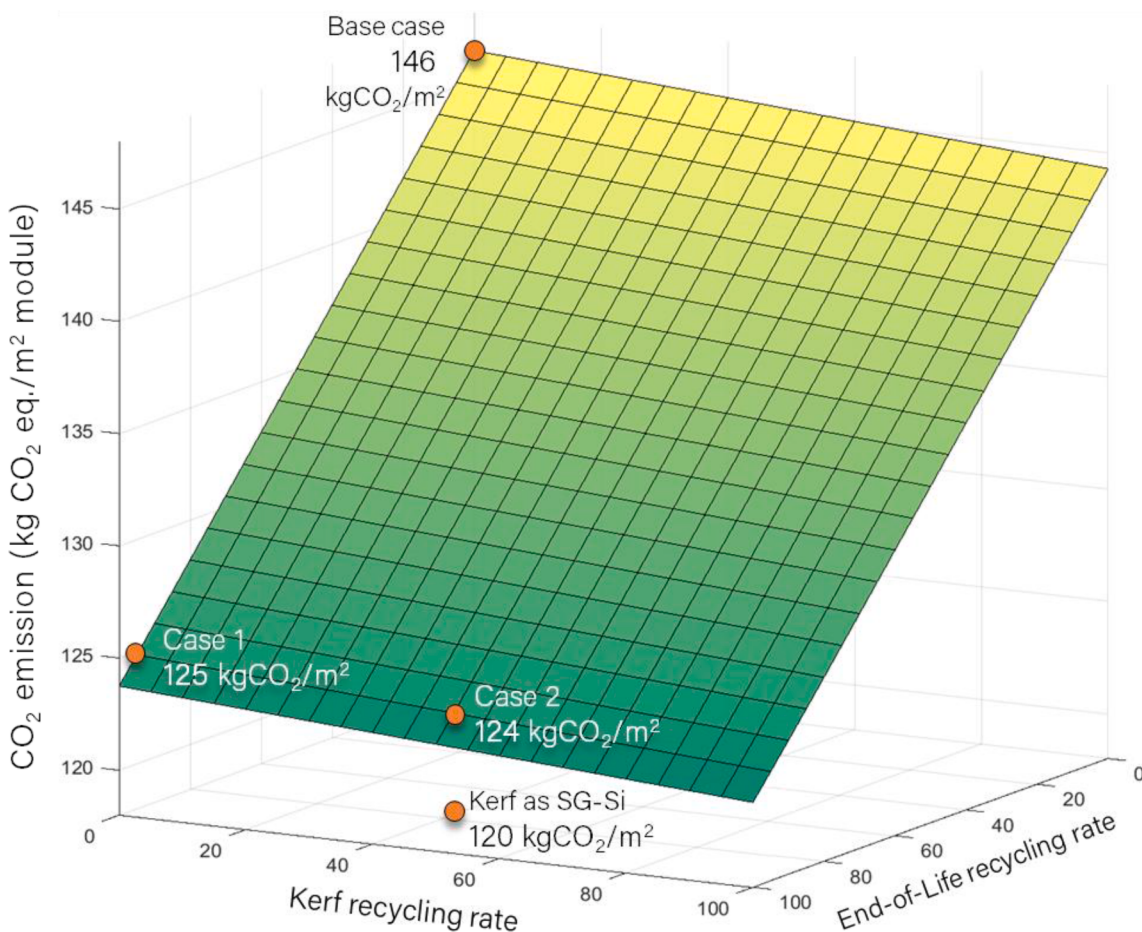
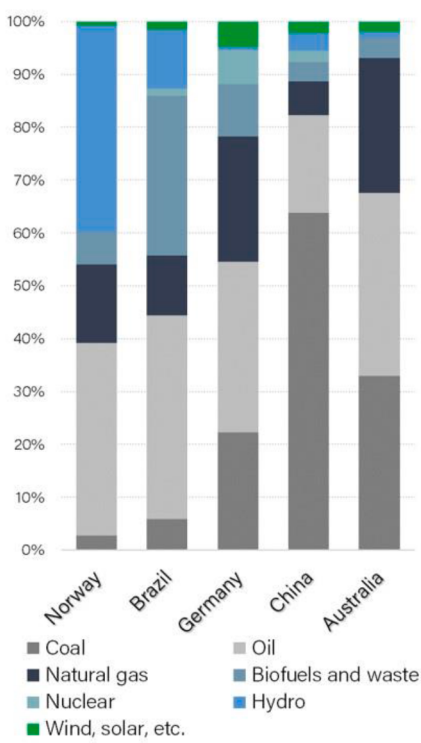


Fig. 9. CO₂-equivalent emission per m² module, with all life cycle steps co-located on the German energy grid.

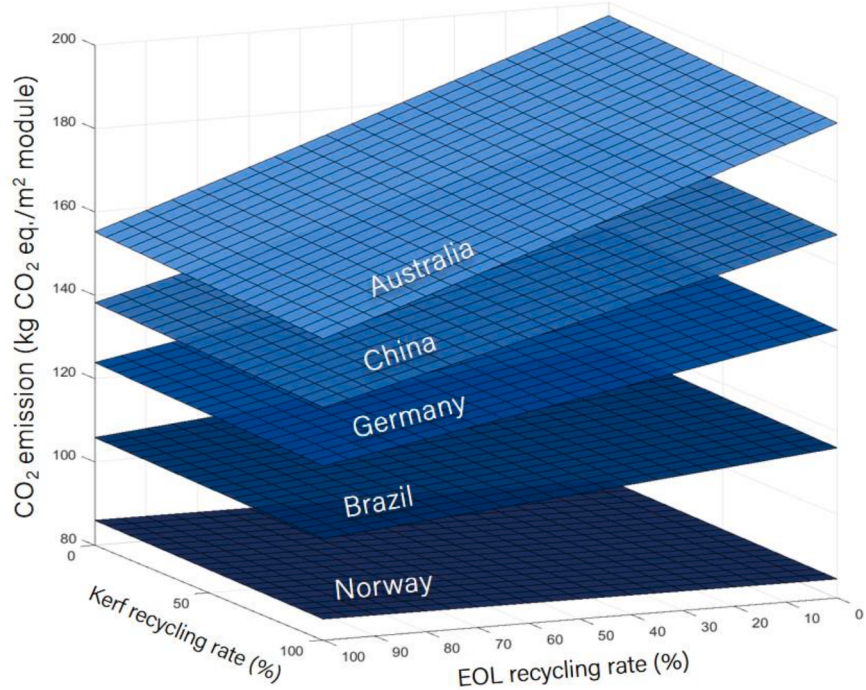
that for the Siemens process.

Systems can be configured to combine any industrially viable technology combinations using the simulation approach. For instance, selecting a recycling process based on polymer pyrolysis rather than combustion would again change the picture as direct CO₂ emissions

would not occur, while at the same time no additional power would be generated from waste heat. The approach presented here offers the flexibility to evaluate and compare the systemic effects of such changes relatively easily, whereas the data for such processes do not exist in the inventory databases as yet.



(a) Energy grid mix compositions



(b) Equivalent CO2 emission

Fig. 10. CO₂ emissions for different energy grid mixes, assuming all life cycle steps are co-located. Based on 2017 data from the IEA (IEA, 2020b).

4. Conclusions

While the elaboration of the PV industry is primarily driven by cost, this study highlights that sustainable CE requires a wider lens. Resource extraction and waste treatment requirements, options for the recovery of secondary resources at high purity, and impacts in all the dimensions of sustainability need to be assessed and optimised if the PV industry is to not just deliver renewable energy, but do so in a sustainable way that does, in fact, facilitate decarbonisation. Industry performance against this goal can only be measured using a highly granular systems approach that considers the full life cycles that PV systems fit into. It is, therefore, recommended that life cycle systems be analysed using rigorous approaches such as that presented in this paper: opportunities for enhancing sustainability and circularity are identified down to the micro level for unit operations, for the processes they are the building blocks of, and the life cycle systems formed by connecting these processes. The non-linear nature of the life cycle is captured in a scalable, deterministic simulation model to predict the effects of various parameter changes on resource requirements and sustainability, to explore performance improvement options, and to compare different processing and design configurations in terms of RC, RE, and carbon footprint. Computational flexibility and efficiency are enhanced by employing NNs as surrogate representations of the simulation. The simulation approach makes it possible to compare and optimise current and future technology options based on up-to-date processes and operating parameters, rather than having to apply aggregated and sometimes outdated information, as is the status quo with most of the general MFA-based LCA approaches.

These methods do not allow for delving into the process specifics of large systems to identify and address the root causes of material and energetic inefficiencies, entropy creation, and environmental emissions.

Simulation results establish the system configurations that would facilitate resource conservation and environmental impact reduction, and quantify the positive impacts of increased circularity on overall sustainability. Both EOL and kerf recycling increase PV module production capacity and hence, nominal PV power generation capacity without the need for additional primary material consumption (Fig. 3). Furthermore, both power consumption and CO₂ emission per module are driven down by increased EOL recycling because of recycled Si bypassing both MG-Si production and SG-Si production via the energy-intensive Siemens process. As kerf recycling only bypasses MG-Si production, its impact is less pronounced. However, if kerf residues were to be upgraded to SG-Si prior to re-entering the value chain, its recycling would provide significant additional reductions in power consumption and CO₂ emission (Figs. 5 and 10). There is a need for continued focus on developing high-value recycling processes for both EOL modules and kerf, on reducing kerf formation and contamination to the minimum practically and economically achievable, and/or eliminating kerf completely through alternative processing techniques e.g. Si deposition methods that eliminate the need for wafer cutting.

Power consumption-related CO₂ emissions (Scope 2) depend strongly on energy grid composition. We highlight the significantly poorer environmental performance of countries that still depend mostly on fossil fuels for power generation (Fig. 10). If energy-intensive production processes are to remain the norm, they should be geographically

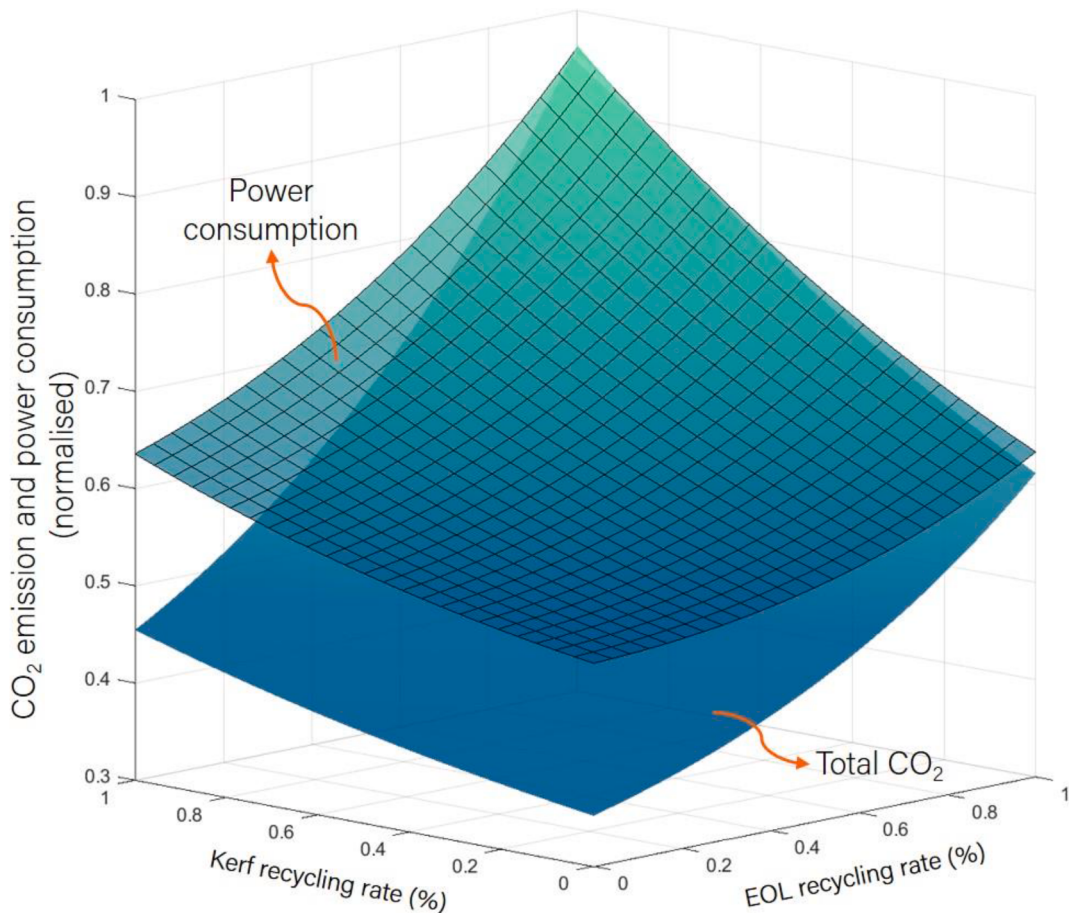


Fig. 11. Variation of power consumption and CO₂ generation (normalised) with recycling rate (Siemens Process SG-Si and Cz mono-Si).

located where energy grids are least dependant on fossil fuels. There is, of course, an economic trade-off to consider but there should be a shift from the primarily *profit*-orientated view to one that strikes a balance between *people*, *planet*, and *profit*. From a policy perspective, instruments such as life cycle carbon pricing likely have a role to play.

From a thermodynamic perspective, Cz crystallisation, wafering, and cell manufacture are the least resource-efficient processes in the closed-loop system (Fig. 7). Further analysis, using exergy cost as a proxy for RC, reveals that the specific causes are Cz crystallisation itself and AlO_x layer deposition, followed by the other cell layer deposition steps. Based on our assumptions in these unit operations, exergy dissipation mainly stems from power consumption without waste heat recovery, and losing materials due to deposition inefficiencies. To limit systemic entropy creation, and by implication the dissipative loss of resources, developing innovations that target these inefficiencies first is recommended.

Simulation results show that, amongst others, Ag and Cu to the value of approximately \$109 and \$55, respectively, can be recovered per tonne of modules recycled (based on 2019 prices). Technoeconomic analyses should be conducted to further explore revenue potential and the trade-offs between high-value recycling at (first) EOL and dismantling for re-use to extend the life cycle and delay recycling. Based on the chosen recycling route, we find that at least 95.5% of Pb introduced via solders can be removed from recycling solutions to prevent potential

release into the environment.

To take advantage of these opportunities, supply chains need to be integrated or designed such that collaboration and quality-focussed recycling are stimulated. In Europe, the WEEE directive and organisations like PV Cycle (pvcycle.org) that facilitate the collection and recycling of EOL modules contribute significantly to these, albeit that WEEE directive targets are largely mass based. Our simulation shows that, by the time EOL modules have been thermally processed (after removal of the frame, glass and polymers, before commencement of metal recovery), current WEEE directive targets have already been exceeded. At the policy level, a shift from mass-based targets to targets for both quantity and quality recycling with respect to specific elements is needed. Policy makers should develop these targets guided by approaches such as that presented here, the contribution of which lies in its agility and its ability to translate the complexities of large non-linear product systems into a consistent physics-based foundation of information. From here, industry and policy makers can:

- make properly informed decisions about future directions for the PV and other industries,
- effectively communicate up-to-date sustainability-related information in a rapidly changing environment (e.g. through the development of performance indicators and labels), and

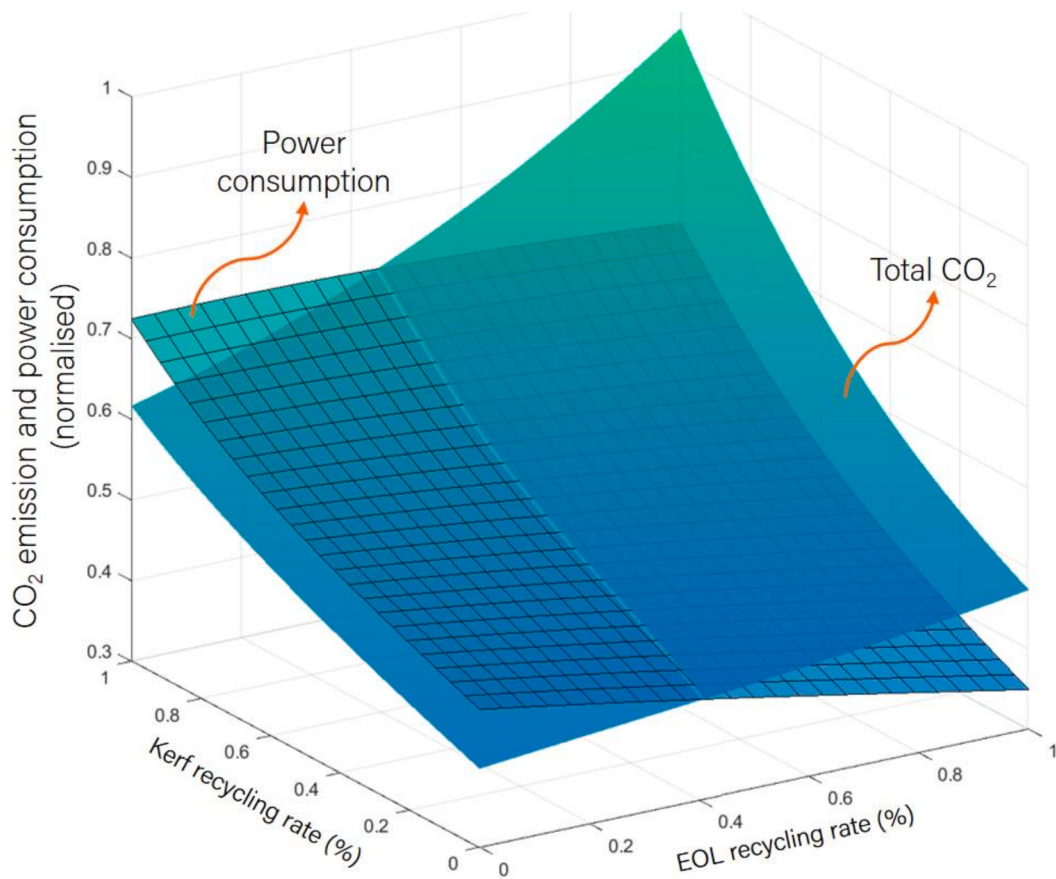


Fig. 12. Variation of power consumption and CO₂ generation with recycling rate (silane FBR SG-Si and mc-Si).

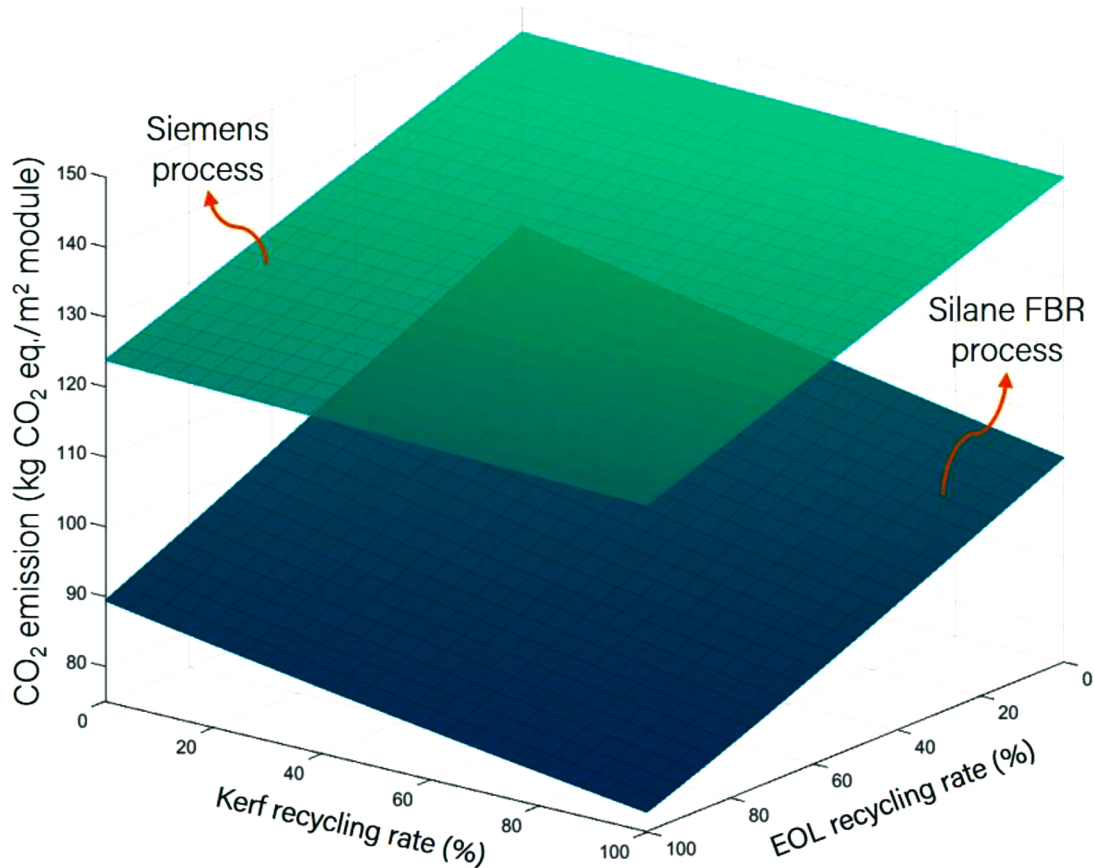


Fig. 13. Variation of CO₂-equivalent emission per m² with recycling rate (note that the top surface is the exact same as that shown in Fig. 9).

- take realistic and impactful operational and regulatory actions to stamp out barriers on the path to maximum sustainability and circularity.

It is, therefore, ideally placed to support decisions regarding decarbonisation, the transformation of global economies to CE, realising the EU Green Deal, and achieving the United Nations' Sustainable Development Goals. It is not limited to the systems covered in this paper, but can be applied to any other PV or complex product system.

5. Outlook

The results presented in this paper are for a static, steady state system based on the current status of the c-Si PV industry. The simulation model can, however, be adopted fairly easily to investigate the systemic effects of technological developments in e.g. wafer size and thickness, materials used, recycling strategy, and so on, as well as projected PV deployment rates, lifetimes and expected waste volumes over time.

We addressed resources and one dimension of sustainability i.e. the environment, and touched on some of the economic benefits of EOL metal recovery. Future work includes the additional assessment of economic and societal impacts, so as to assess and optimise the system across all three dimensions of sustainability.

We alluded to the fact that this approach can be applied to other systems. Significant R&D currently focusses on the development of tandem PV technologies that better exploit solar energy to bring about step changes in PCE. In particular, the development of perovskite-based PV is gaining significant traction. As such, the simulation of c-Si/

perovskite tandem PV systems is currently underway. The methodology is being expanded to also include technoeconomic assessments and the optimisation of sustainability and circularity.

Credit author statement

Neill Bartie: Conceptualization, Methodology, Software, Validation, Formal Analysis, Investigation, Writing – Original Draft, Visualization; **Lucero Cobos-Becerra:** Conceptualization, Validation, Investigation, Writing – Original Draft, Writing – Review & Editing, Visualization, Project Administration; **Magnus Fröhling:** Conceptualization, Validation, Writing – Review & Editing, Supervision; **Rutger Schlatmann:** Conceptualization, Methodology, Validation, Writing – Review & Editing, Supervision; **Markus Reuter:** Conceptualization, Methodology, Software, Validation, Writing – Review & Editing, Supervision.

Declaration of Competing Interest

The authors declare that they have no known competing financial interests or personal relationships that could have appeared to influence the work reported in this paper.

Acknowledgements

The authors would like to thank Dr. Christina Meskers and two anonymous reviewers for their constructive contributions to enhancing the quality of this paper.

6. Appendix A

6.1. Methods

Fig. A1.1 shows a schematic representation of such a network and its relation to the process simulation.

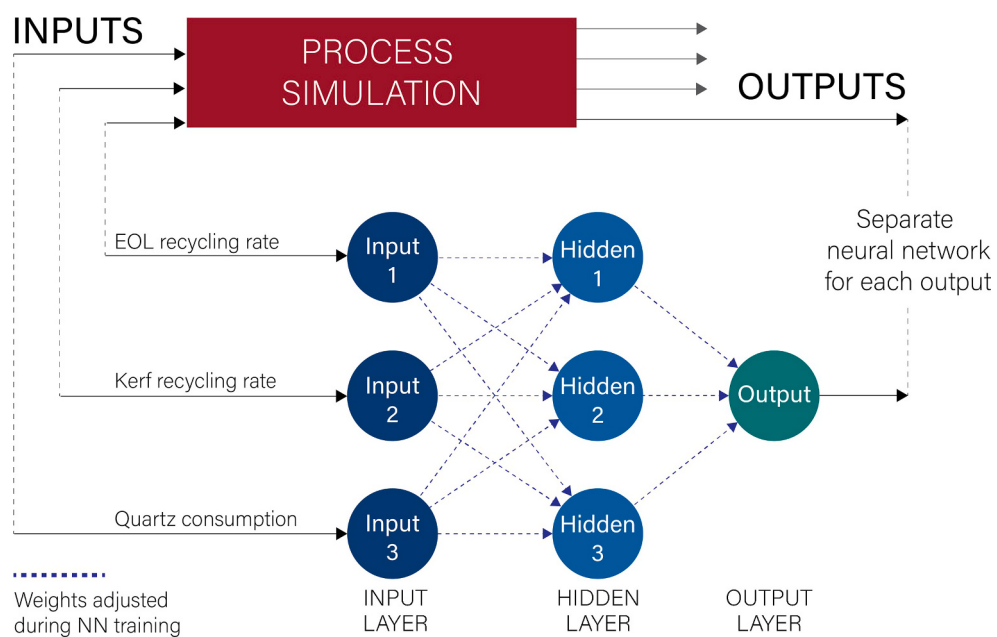


Fig. A1.1. Neural network structure and links to process simulation in/outputs (note that hidden and output layers each have a bias neuron, which are not shown).

6.2. Process Descriptions and Assumptions

The simulated life cycle consists of 75 process units and 333 process streams containing 155 compounds. The main process steps and assumptions are briefly described here.

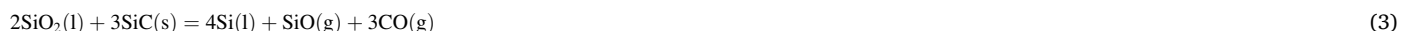
6.3. Metallurgical grade silicon

Metallurgical grade silicon (MG-Si) is produced by the carbothermic reduction of silica (SiO_2). Quartzite sand is smelted in an electric arc furnace (EAF) with a number of other materials essential to the process (e.g. coke, charcoal, and woodchips) (Zulehner et al., 2000; Øvreliid and Pizzini, 2017).

As quartz (SiO_2) melts in the cooler zones (below about 1835 °C), it reacts with carbon to form silicon carbide (SiC), which acts as the reductant in producing the final silicon metal, according to reactions (1) and (2).



In the high-temperature zone in close proximity to the electrodes (at 1900–2100 °C), reactions (3) and (4) take place (PCC, 2017) to produce crude silicon at a typical yield of between 80 and 90% (Ciftja et al., 2008), and a gas phase containing primarily CO, SiO and H_2O . For the purposes of our simulation, we assume a yield of 85%.



Any SiO(g) that enters the offgas stream reacts according to reaction (5) to form a silica fume.



The fume byproduct—microsilica—is captured in the gas cleaning system and sold as a valuable additive in the construction and refractory industries (Ciftja et al., 2008). Crude silicon purity is typically 96 to 99% depending on the quality of raw materials and EAF electrodes used. The main impurities dissolved in the metal phase are given in Table A2.1 (Ceccaroli and Lohne, 2011).

Further purification is achieved through ladle refining, during which the addition of slagging agents such as SiO_2 and CaO allow for impurities less noble than Si (e.g. Al, Ca and Mg) to be oxidized. Temperature is maintained by blowing oxygen through the melt, leading to the exothermic oxidation of Si, so resulting in a loss of product Si. The reactions involved are listed below, with underlined elements dissolved in metal, and those in parentheses dissolved in slag (Ceccaroli and Lohne, 2011).



Gibbs free energy minimization is used to estimate the thermodynamic equilibrium distributions of Al, Ca and Mg between the metal and slag phases. Carbon, in the form of suspended SiC particles, is also removed with ladle slag. Some dissolved C remains in the metal phase, however, at levels between 100 and 600 ppm (Ceccaroli and Lohne, 2011; Kakalashe and Tangstad, 2011). Our simulation gives a value of 182 ppm.

Boron (B) and Phosphorous (P) are electrically active elements that need to be removed to ultimately be added back into high-purity Si as dopants in carefully controlled quantities during PV cell manufacture. Boron is removed during ladle refining according to reaction 10 (Safarian et al., 2012).



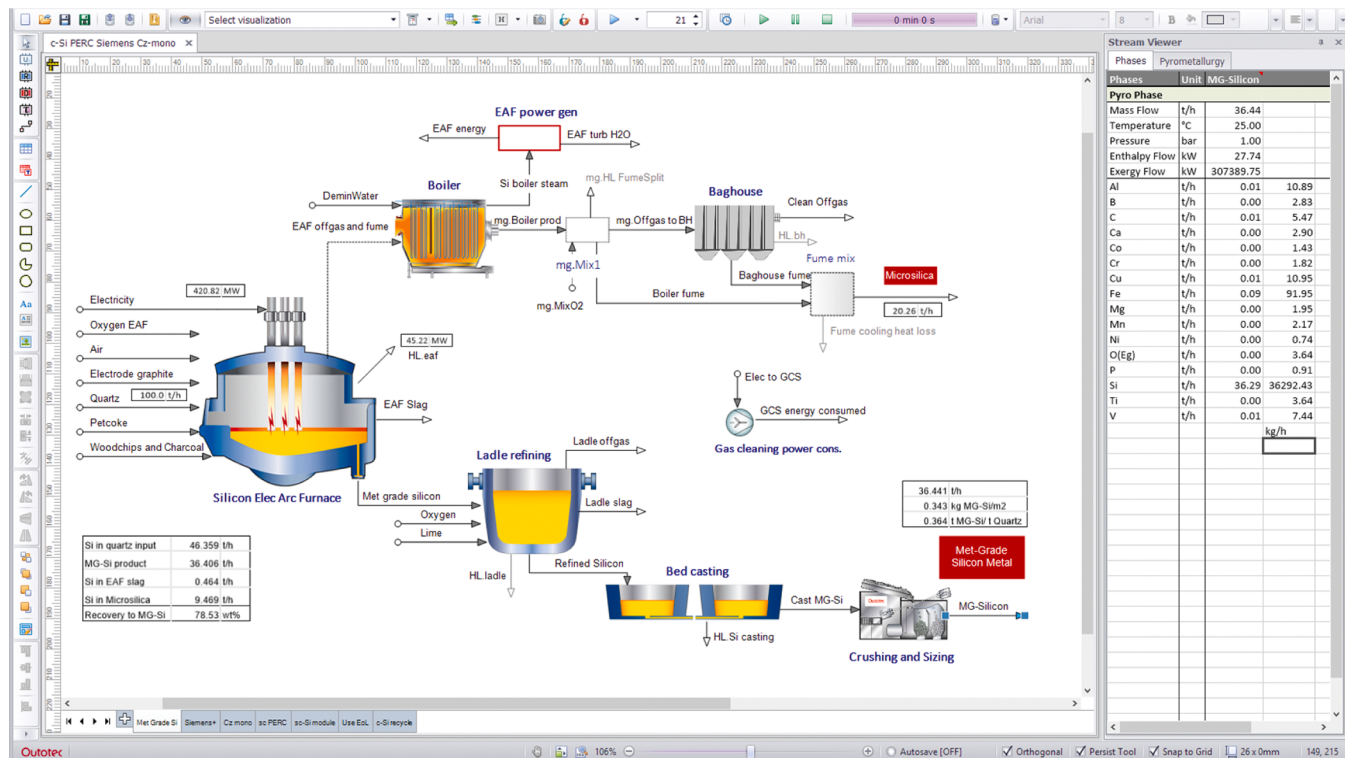
The removal of B via ladle refining can be affected negatively by the presence of Al_2O_3 in the slag (Jakobsson and Tangstad, 2014). Applying these authors' findings, the refining slag Al_2O_3 content in our simulation results in a residual B content of 78 ppm in the metal phase. We assume a final P concentration of 25 ppm (Miki et al., 1996). The distributions of other contaminants are calculated such that the final product composition agrees with those in various academic publications (e.g. Kakalashe and Tangstad, 2011; Ceccaroli and Lohne, 2011; Zulehner et al., 2000; Øvreliid and Pizzini, 2017). After ladle refining, slag is removed and the refined Si metal is cast into ingots, cooled, and then crushed and sized. The process simulation flowsheet is shown in Fig. A2.1.

The quantities and compositions of feed materials and EAF electrodes relative to the input amount of quartzite are taken from literature, both academic and industrial (PCC, 2017; Zulehner et al., 2000; Chigondo, 2018; Chandrasekaran et al., 2012). EAF specific energy consumptions reported in the literature range from 11 to 14 MWh/t of metal produced (Zulehner et al., 2000; Kakalashe and Tangstad, 2011). We deduce a value of 11.4 MWh/t from information published by PCC Bakkisilicon hf. (PCC, 2017) and estimate power consumption and heat losses based on expected product temperatures and a closed energy balance. Heat is partially recovered from the hot offgas stream, and is used to generate electricity, which reduces the primary energy demand. Product, residue and direct emission (e.g. carbon dioxide) quantities are calculated from the chemical and physical transformations described above, validated and adjusted as appropriate to match industrial reality while maintaining closed mass balances.

Table A2.1

Impurities in crude metallurgical grade silicon.

Iron (Fe)	0.2 – 3 wt%	Titanium (Ti)	0.01 – 0.1 wt%
Aluminium (Al)	0.4 – 1 wt%	Carbon (C)	0.1 – 0.15 wt%
Calcium (Ca)	0.2 – 1 wt%	Oxygen (O)	0.01 – 0.05 wt%
V, Cr, Mn, Co, Ni, Cu, Zr and Mo	tens to hundreds of ppm(w)	B, P	10 – 100 ppm(w)

**Fig. A2.1.** Simulation flowsheet for metallurgical grade silicon production.

6.4. Solar grade silicon

Most manufacturers adopt the established, but energy intensive, Siemens process for polysilicon production. Process improvements have led to energy consumption decreasing from 200 kWh/kg Si in 2009 (Yan, 2017) to around 71 kWh/kg Si in 2018 (IEA PVPS, 2019). To date, less than 5% of manufacturers have adopted the far more efficient FBR process, which consumes significantly less energy (around 10 kWh/kg Si) (IEA PVPS, 2019). Furthermore, tariffs and trade tensions between the USA and China have put producers under pressure—REC Silicon, for example, in an effort to maintain liquidity, has had to halt FBR operations at its Moses Lake production facility due to insufficient access to Chinese polysilicon markets (REC, 2019). Nonetheless, greater adoption of lower-energy processes would reduce energy payback time (EPBT), a PV performance indicator that measures the time required for a PV system to generate the amount of energy consumed for its manufacture, so increasing sustainability. For the main simulation of this life cycle stage, the Siemens Process is used. The simulation flowsheet is shown in Fig. A2.2.

MG-Si is reacted with hydrogen chloride (HCl) in a FBR at temperatures between 300 and 500 °C and pressures between 1 and 5 bar to produce trichlorosilane (TCS - SiHCl₃) and some silicon tetrachloride (STC - SiCl₄) (Bye and Ceccaroli, 2014) according to reactions (11) and (12).



A selectivity of 90% towards TCS, the desired product, is achieved by adding a 10% excess of HCl (Ramírez-Márquez et al., 2018). It is assumed that MG-Si impurities exit the system in this step with unreacted Si (assumed to be 5% of input Si) and in the offgas stream. In order to estimate HCl consumption more accurately, the compounds formed from the impurities are predicted using Gibbs free energy minimisation in FactSage (GTT-Technologies, 2020) and are as follows:

Solid phase: FeCl₂, MnCl₂, CaCl₂, MgCl₂, CrCl₂, Cu₃P, VCl₂, Co₂P, and Ni₅P₂

Gas phase: AlCl₃, BCl₃, TiCl₄

TCS is subsequently separated from STC and further purified in two fractional distillation steps. Si deposition takes place in a Siemens chemical vapour deposition (CVD) reactor, in which TCS is diluted in pure hydrogen (H₂) to decompose and deposit SG-Si onto pure Si filaments at 1000–1100 °C (Jiao et al., 2011; Safarian et al., 2012).

The main reactions that occur in the deposition reactor are as follows (Ceccaroli and Lohne, 2011):

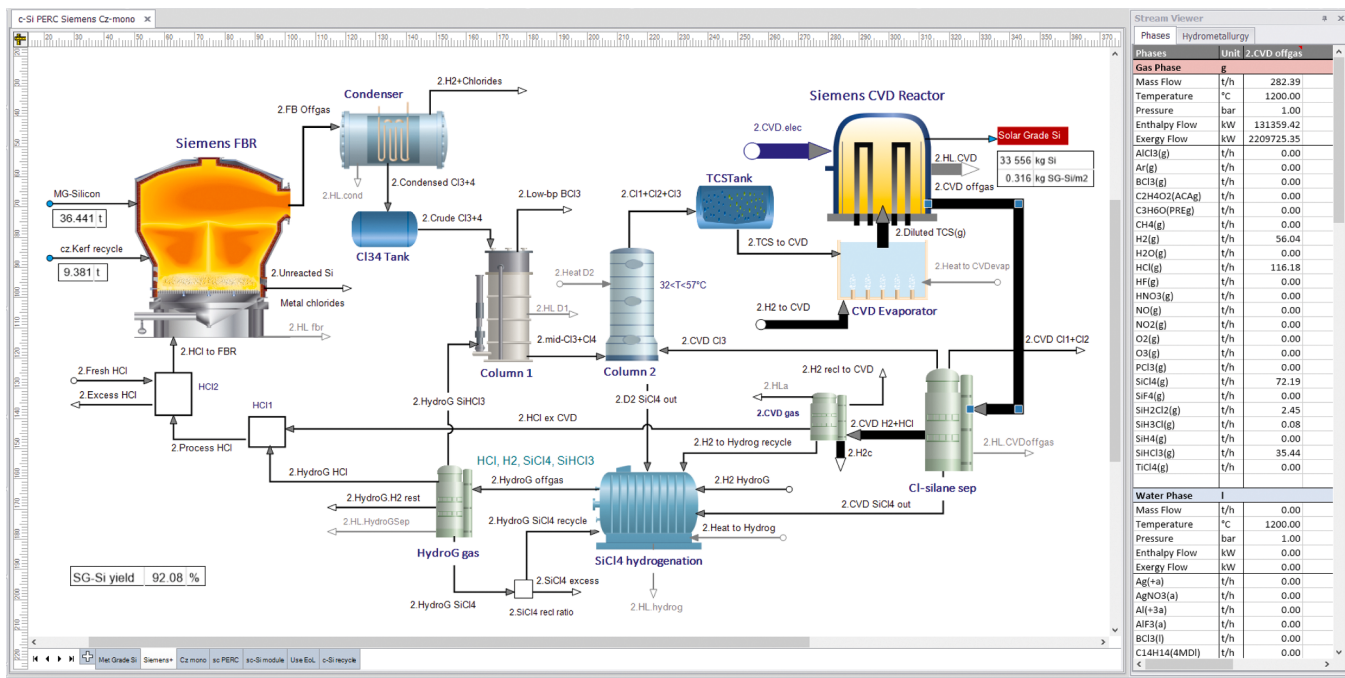


Fig. A2.2. Simulation flowsheet for solar grade silicon production via the Siemens process.



The offgas stream, therefore, contains SiHCl_3 , SiH_2Cl_2 , SiCl_4 , HCl , and H_2 , and we use Gibbs free energy minimisation to estimate the amounts of each exiting the CVD reactor. To improve process efficiency, STC is recycled by converting it into TCS by hydrogenation, according to reaction (17) (Seigneur et al., 2016).



As mentioned earlier, the process is energy intensive and inefficient with significant dissipative losses (Ceccaroli and Lohne, 2011). We assume an overall power consumption of 95 kWh/kg SG-Si produced but acknowledge that modern facilities achieve 71 kWh/kg, as mentioned in the Introduction. Depending on the case being investigated (refer to Table 1), kerf residue may re-enter the process here with MG-Si. All of the SG-Si produced is transferred to the next process for the production of mono-Si wafers.

In Section 3.4, a comparison is made with the alternative SG-Si production route mentioned earlier—the production of silane (SiH_4) from MG-Si and the subsequent production of granular SG-Si in a FBR. Silane is produced via the disproportionation of trichlorosilane (SiHCl_3), which involves the reaction of MG-Si with hydrogen (H_2) and silicon tetrachloride (SiCl_4) to produce SiHCl_3 , and the subsequent catalytic redistribution of purified SiHCl_3 in fixed bed columns (Bye and Ceccaroli, 2014). In the silane FBR, seed particles of pure Si are fluidized in a preheated stream of SiH_4 and H_2 . The SiH_4 decomposes unidirectionally into Si and H_2 , and Si deposits on the seed particles, which grow until their weight causes them to fall out of the fluidized bed (Jiang et al., 2017). This process consumes 80–90% less electricity than the Siemens process and is a continuous rather than a batch process, which offers several advantages (Jiang et al., 2017) amongst which is significantly lower CO_2 (Scope 2) emissions. Detailed descriptions of these processes can be found in the cited references.

6.5. Monocrystalline silicon ingots and wafers

The Cz method is used to produce mono-Si ingots from which Si wafers are sawn. The process (depicted in Fig. A2.3) starts with the cleaning of Si feedstock and the removal of SiO_2 by etching in an acid bath consisting of a mixture of nitric (HNO_3), hydrofluoric (HF) and acetic (CH_3COOH) acids (Hirtz et al., 1992). The general etching reactions are:



The role of acetic acid in the solution is as a diluent, oxidation promotore, and a wetting agent (Yifan et al., 2013). The quantities of reagents and products for this step are calculated using reactions (18) and (19) above and the HNA volumetric ratio of HF:HNO₃:CH₃COOH = 1:6:1 reported by Yifan et al. (2013). The offgas stream is cleaned in a scrubber where sodium hydroxide (NaOH) is used to remove NO_x, HF, HNO₃ and CH₃COOH (Jungbluth et al., 2010). The resulting effluent contains sodium nitrate (NaNO₃), sodium fluoride (NaF) and sodium acetate (NaCH₃COO) and is transferred to a water treatment unit. After a rinsing step in deionised (DI) water and drying with acetone (CH₃COCH₃), the Si feedstock proceeds to

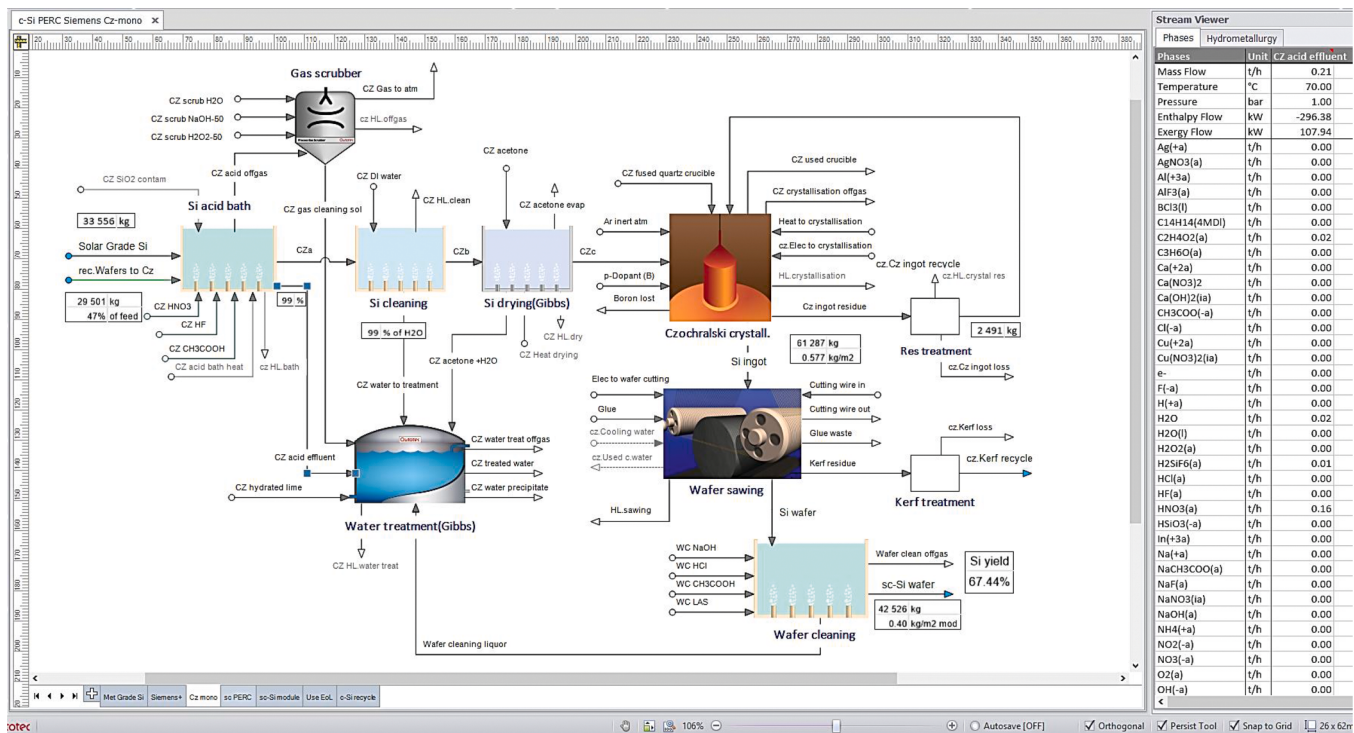


Fig. A2.3. Simulation flowsheet for Czochralski crystallisation and wafer cutting, showing some of the aqueous species tracked in the simulation, in the table on the right hand side (here showing some quantities for the acid bath effluent liquor).

the Cz crystallisation step.

Conventional Cz crystallisation of a mono-Si ingot entails melting the Si feedstock and controlled amounts of the required dopant (B in this case for a p-type ingot) in a quartz glass crucible, dipping a single crystal seed into the melt, and withdrawing it from the melt following carefully controlled speed and temperature profiles to start growing a cylindrical mono-Si ingot of the required diameter (Seigneur et al., 2016). Boron is added to achieve a dopant concentration of $1 \times 10^{16}/\text{cm}^3$ (Rodriguez et al., 2011), assuming a 50% loss of B during the process. The crucible is consumable and is lost together with some remaining solidified Si residue (Dold, 2015), while the susceptor can be reused for a number of cycles (Lan et al., 2009). The furnace chamber is flushed with argon (Ar) for the entire duration of the cycle to continuously remove SiO gas that forms as a result of contact between the melt and the quartz crucible, so preventing SiO₂ deposition in the furnace chamber (Dold, 2015) and lowering the risk of particulates falling into the melt, which could cause dislocations in the crystal, necessitating a restart of the growth process (Lan et al., 2009). Power consumption for the crystallisation process is taken as 33 kWh/kg crystal (VDMA, 2020).

Diamond wire sawing is used to cut wafers with a thickness of 170 µm (VDMA, 2020). The wire consumption rate is estimated using a wire performance of 250 cm²/m (wafer area cut per metre of wire consumed) and a wire thickness of 120 µm (Peguirón et al., 2014). Kerf residue represents the largest and most expensive material inefficiency in the system with approximately 32% of mono-Si lost with a kerf thickness of 75 µm (VDMA, 2020). Recent European projects such as CABRISS (www.spire2030.eu/cabriiss), amongst others, have demonstrated successful kerf recycling, achieving purities of up to 4 N, albeit with a requirement to manage a number of safety concerns (Halvorsen et al., 2017). Ongoing research projects like SELISI (selisi.eu) and collaboration with private companies aim to further this work, indicating that module and kerf recycling remain priorities from both industry and policy perspectives. ROSI Solar, for instance, has been one of the first to be awarded funding for their work in this field under the EU Green Deal (ROSI Solar, 2020). Furthermore, with Si metal listed as a critical metal and the forecast growth in the PV and other Si-consuming industries like electronics and batteries, future shortages of high purity metal may occur. For these reasons, kerf recycling is one of the main topics investigated in this paper.

After sawing, wafers are etched to remove surface damage and cleaned to remove any residues (Rodriguez et al., 2011). Reagent and energy consumptions for this step are estimated from Jungbluth et al. (2010) and Frischknecht et al. (2015). Finally, all acidic liquors from the crystallisation and wafering processes are neutralised in a water treatment unit using hydrated lime (Ca(OH)₂). All of the wafers produced in this process are transferred to the cell manufacturing process.

6.6. Cell manufacture

The PERC solar cell architecture (shown in Fig. A2.4a) uses an advanced silicon cell architecture, the key improvement being the integration of a back-surface passivation layer. This layer of material on the back of the cell that is able to improve its PCE to between 21% and 24%, compared to 18 to 19% for conventional aluminium back surface field (Al-BSF) cells (Blakers, 2019). The passivation layer increases the overall cell efficiency in three key ways: (i) it reduces rear-side recombination losses; (ii) it increases the absorption of light and (iii) it enables higher internal reflectivity (Allen et al., 2019; Blakers, 2019; Mandal et al., 2020). In line with current PV industry and market trends, the PERC cell design is used in our simulation. The process steps in our simulation follow, for the most part, those described by Werner et al. (2017) and are shown in Figs. A2.4b and A2.5. Based on industry trends (VDMA, 2020), we consider cells 166 mm in length and 166 mm in width (size M6). Indication are, however, that larger M12 (210 mm x 210 mm) cells may gain market share sooner than expected (e.g. PVTECH, 2020a, 2020b), in which case it would be relatively straightforward to modify wafer size and to rerun our simulations.

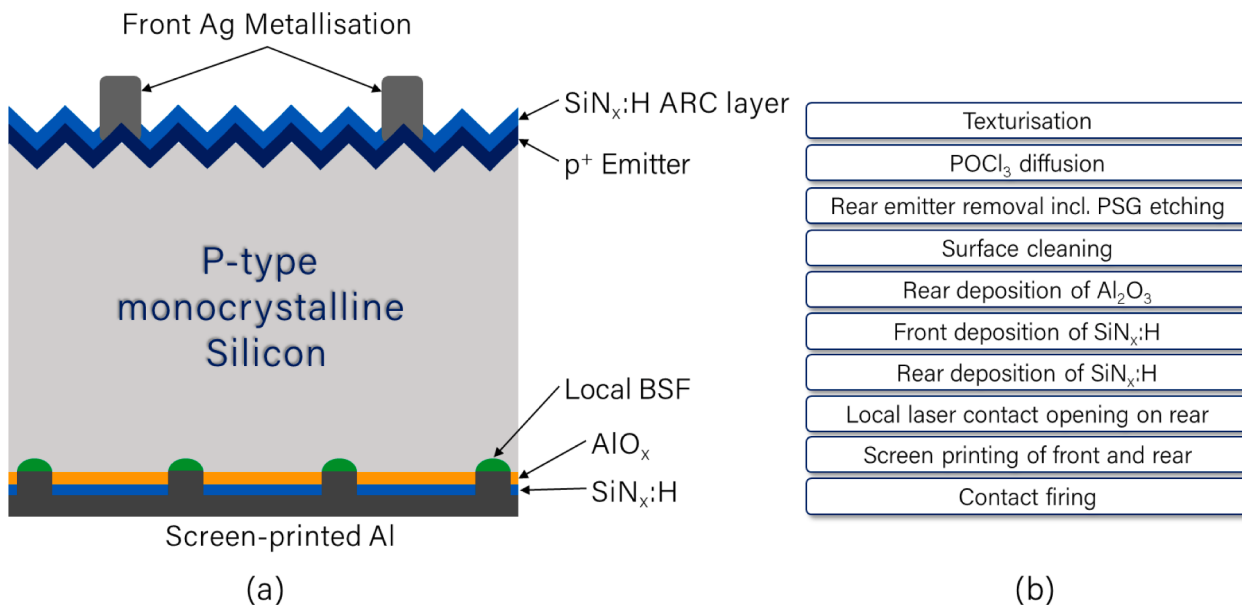


Fig. A2.4. (a) Passivated emitter rear contact (PERC) PV cell architecture, and (b) production steps.

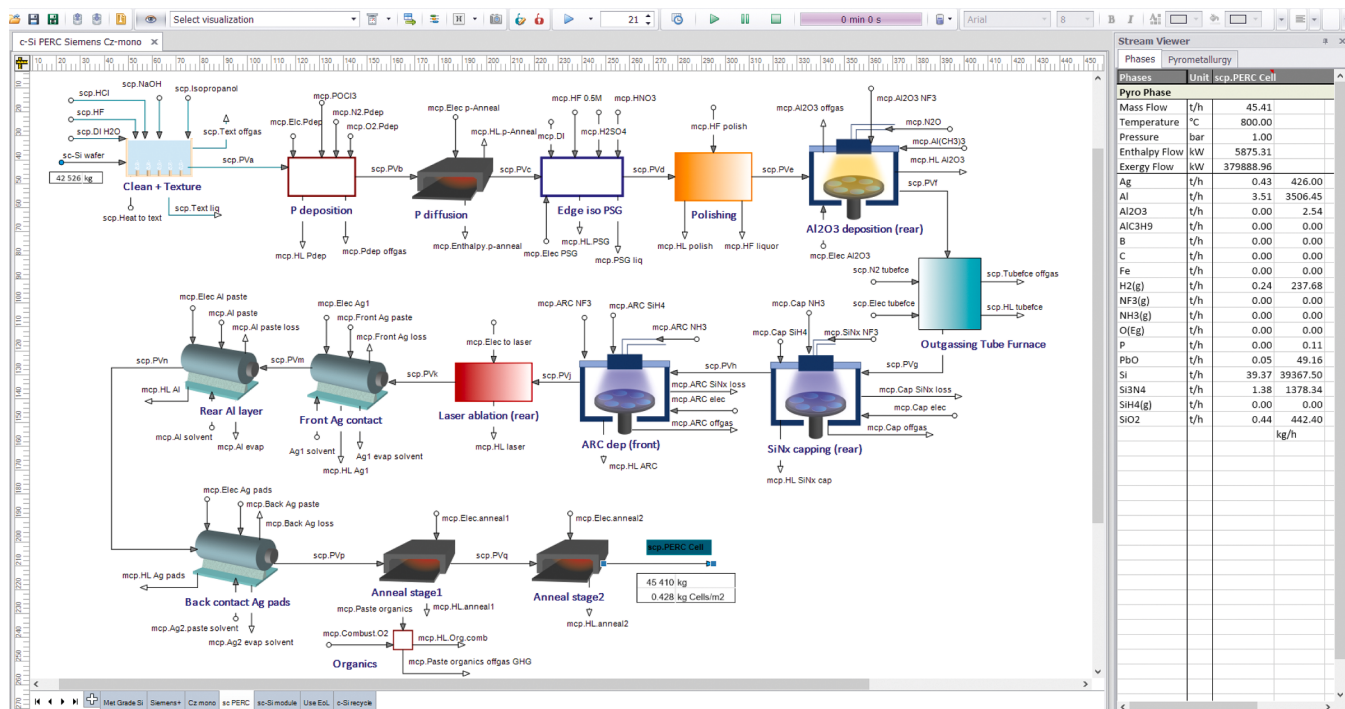
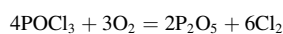
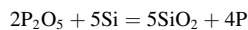


Fig. A2.5. Simulation flowsheet for PERC PV cell manufacturing showing mass, element, compounds, enthalpy, and exergy flows.

The process starts with the cleaning and texturing of the wafers produced in the previous step. Etching in HNO₃ and HF removes approximately 5 µm of Si on either side of the wafer, followed by a cold KOH etch to remove a thin layer of remaining porous Si. Further washing and etching steps (in HCl, HF and DI water) remove remaining residues (Hahn and Joos, 2014). The consumptions of HNO₃ and HF are calculated from the volume of Si to be etched and the etching reactions. Water consumption is taken as 33.4 L/m² wafer (Louwen et al., 2015) and other reagent consumptions are based on inventory data reported by Frischknecht et al. (2015). Energy requirements are determined by closing the energy balance. Products and effluents from this step include NO, H₂SiF₆, unused HCl, HNO₃, HF, KOH, isopropanol and used DI water.

During the next group of steps, the P-doped homogeneous emitter is deposited. The dopant precursor, phosphorous oxychloride (POCl₃), reacts with O₂ at 830 °C (Li et al., 2017) to form P₂O₅ and Cl₂. The O₂ oxidises the wafer surface, and the resultant SiO₂ - P₂O₅ combination forms a phosphor-silicate glass (PSG) layer, which then acts as the actual dopant source (Hahn and Joos, 2014). Relevant chemical reactions used in our simulation are:



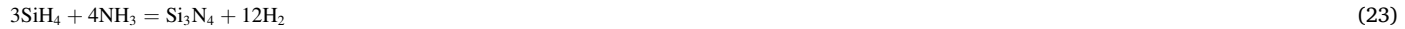


The deposited dopant is subsequently driven further into the silicon through annealing in the absence of POCl_3 (Li et al., 2017). We assume an active doping depth of 1 μm (Hahn and Joos, 2014) and an average P concentration of $10^{19}/\text{cm}^3$ in the active volume to calculate the POCl_3 consumption and PSG formation according to reactions 15 and 16. The PSG layer on the front surface is removed using dilute HF and the emitter deposited on the rear of the wafer in a wet etching process which involves the use of H_2O , HF, HNO_3 , and H_2SO_4 (Hahn and Joos, 2014). A further polishing step takes place in a dilute (1% in H_2O) HF solution (Dingemans et al., 2010). Products and effluents from this step include POCl_3 , O_2 , N_2 , P_2O_5 , Cl_2 , P , SiO_2 , H_2SO_4 , HNO_3 , HF, and used DI water.

Rear passivation is achieved through PECVD of a 6 nm AlO_x (expressed as Al_2O_3) layer (Werner et al., 2017) with $\text{Al}(\text{CH}_3)_3$ as the precursor according to reaction 22 (Hofmann et al., 2013).



After an outgassing step using N_2 , the Al_2O_3 layer is capped with a 100 nm (minimum) layer of SiN_x (expressed as Si_3N_4), deposited by PECVD. Similarly, a 75 nm SiN_x layer deposited on the front surface serves as both a passivation and an anti-reflective layer (Werner et al., 2017). The precursors for the SiN_x layer are SiH_4 and NH_3 , which form Si_3N_4 according to reaction 23.



PECVD deposition efficiency is assumed to be 25% and deposition chambers are cleaned using NF_3 gas (Louwen et al., 2015). The main products and effluents from the PECVD steps are Al_2O_3 , $\text{Al}(\text{CH}_3)_3$, N_2O , NF_3 , NH_3 , SiH_4 , Si_3N_4 , N_2 . Because the GWP of NF_3 gas is 16,100 times that of CO_2 (Greenhouse Gas Protocol, 2016), it is extracted from the offgas stream and does not contribute to Scope 1 emissions in our simulation.

The PERC-specific local contact openings are then created by laser ablation. Metallization of the front (busbar grid) and rear surface (Ag and Al, respectively), and the rear contact pads (Ag) are achieved by screen printing. Dry metallization pastes are assumed to contain 80 wt% of the relevant metal (Ag or Al), 10 wt% glass frit, and 10 wt% organic binders (Hahn and Joos, 2014) and pastes are assumed to contain 30 wt% solvent, which is taken to be butyl acetate ($\text{C}_6\text{H}_{12}\text{O}_2$) (Gong et al., 2015). Total paste consumptions (including losses during manufacturing) are calculated from VDMA (2020).

After drying and the evaporation of the solvents at 150–200 °C, curing takes place following a firing program that removes the organic binders (below 600 °C) and forms the Ag and Al contacts following a temperature profile up to 800 °C before cooling and recrystallization (Hahn and Joos, 2014). Typical power consumptions for wet etching, PECVD, screen printing and annealing are taken from Louwen et al. (2015).

6.7. Module assembly

PV module assembly commences with cleaning of the glass substrate, and the preparation of fluxed Sn-coated Cu ribbons, which are used to string sets of 10 to 12 cells together by soldering (Wirth, 2013). After placing the first EVA encapsulant layer with a thickness of 450 μm (VDMA, 2020) on the glass substrate, 5 or 6 cell strings are placed and soldered together in series. Another encapsulant layer is then placed, followed by the back sheet, which consists of a layer of PET (250 μm) sandwiched between two layers of PVF (40 μm each), the so-called TPT configuration (Blieske and Stollwerck, 2013; Frischknecht et al., 2015). The completed layup is then laminated under vacuum at 150 °C. After cooling, module edges are trimmed and sealed using PVB, the module is framed with an aluminium alloy (AlMg_3) frame, and the junction box is attached (Wirth, 2013). As a final step, the module is tested. The process is depicted in Fig. A2.6.

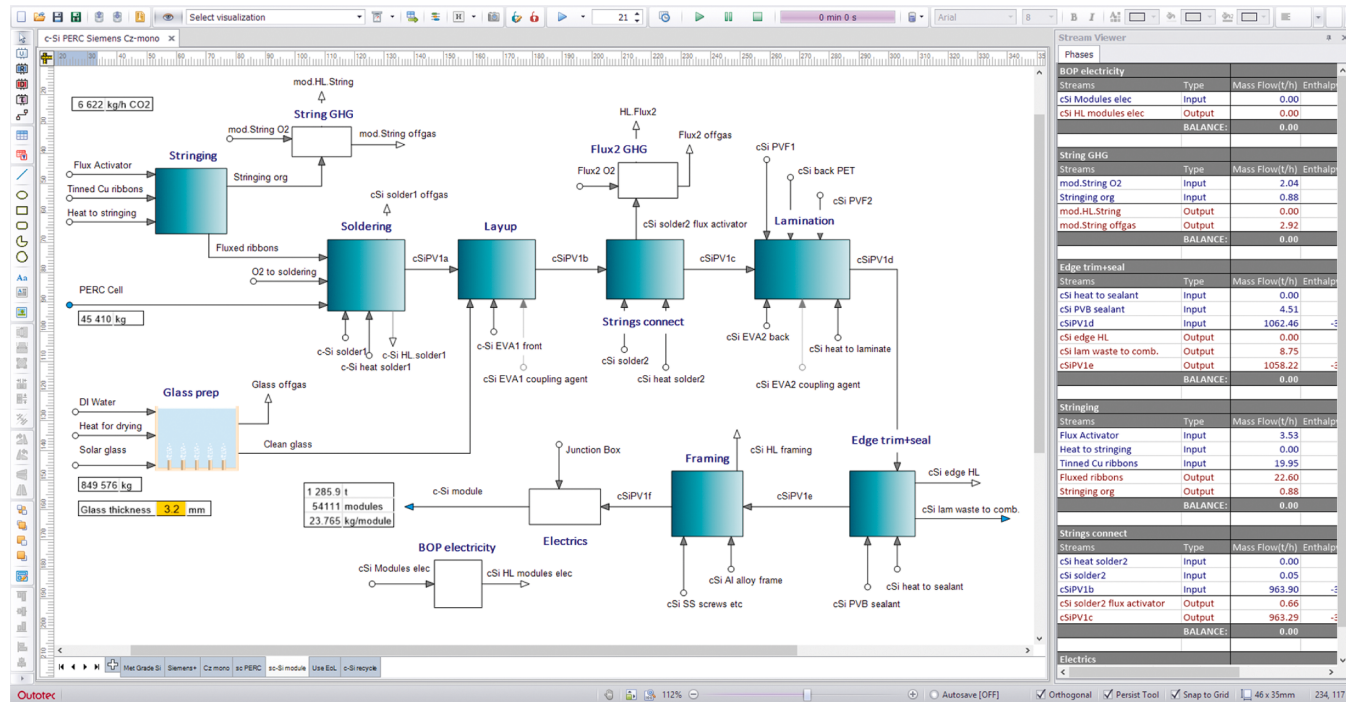


Fig. A2.6. Simulation flowsheet for PV module assembly steps.

We use the following additional parameters based on the cited references:

- Module dimensions are 1981 mm x 991 mm ([energysage, 2020](#)).
- Each module contains 72 cells ([Frischknecht et al., 2015; VDMA, 2020](#)).
- Glass thickness is 3.2 mm ([Frischknecht et al., 2015](#); VDMA, (2020) specifies >3 mm).
- Solder type Sn63 (63 wt% Sn, 37 wt% Pb) is used throughout, and its consumption is deduced from the aggregated data provided by [Frischknecht et al. \(2015\)](#).
- The soldering flux activator and solvent are assumed to be adipic acid and isopropanol, respectively ([Wirth, 2013](#)), and are included for the purposes of estimating potential environmental impacts.
- Total power consumption is calculated using the specific consumption (3.73 kWh/m² module) reported by [Frischknecht et al. \(2015\)](#).

6.8. End-of-life module recycling

Under the European Waste Electrical and Electronic Equipment (WEEE) Directive (2012/19/EU), at least 85% of the PV modules put on the market shall be collected, and at least 80% “prepared for reuse and recycled” ([European Union, 2012](#)). Other than landfilling, dominant recycling approaches for c-Si PV modules involve their treatment in general recycling facilities with other waste electronic goods or laminated glass ([Dufou et al., 2018](#)). With these, the mass-based targets of the directive can be met without having to pay considerable attention to the quality of recyclates and as a consequence, components like Ag, Cu, Si, and Pb are lost and their potential environmental impacts not mitigated ([Heath et al., 2020](#)). More sophisticated, PV-dedicated upcycling processes generally consist of two main steps: (i) module delamination, achieved through mechanical, thermal, or chemical methods, and (ii) cell recycling, consisting of wafer/metal separation to recycle Si, and the subsequent extraction of metals ([Deng et al., 2019](#)). [Heath et al. \(2020\)](#) identify the FRELP¹ ([Latunussa et al., 2016](#); [Ardente et al., 2019](#)) and ASU² ([Huang et al., 2017](#)) processes to have the potential to advance PV recycling. Despite not recovering the whole suite of minor elements in the c-Si system, these aim to integrate the delamination and cell recycling steps and achieve high recoveries of Ag, Cu, Al, Si, glass, and insulated cable ([Heath et al., 2020](#)).

For this study, the recycling simulation (depicted in Fig. A2.7) consists of dismantling, thermal de-encapsulation and glass separation, polymer combustion, string dissolution and metal recovery, wafer etching, and neutralisation of the leach liquors. Dismantling involves the removal of the junction box and frame and the thermal processing step involves the separation of the glass, backsheets, and polymer layers from the cell strings. Glass is assumed to be recovered intact, but is not recycled directly into new modules in the current simulation. The metal and wafer recovery steps follow that proposed by [Huang et al. \(2017\)](#), i.e. the ASU process. It was selected because of its ability to recover Si at SG-Si quality and its self-limiting

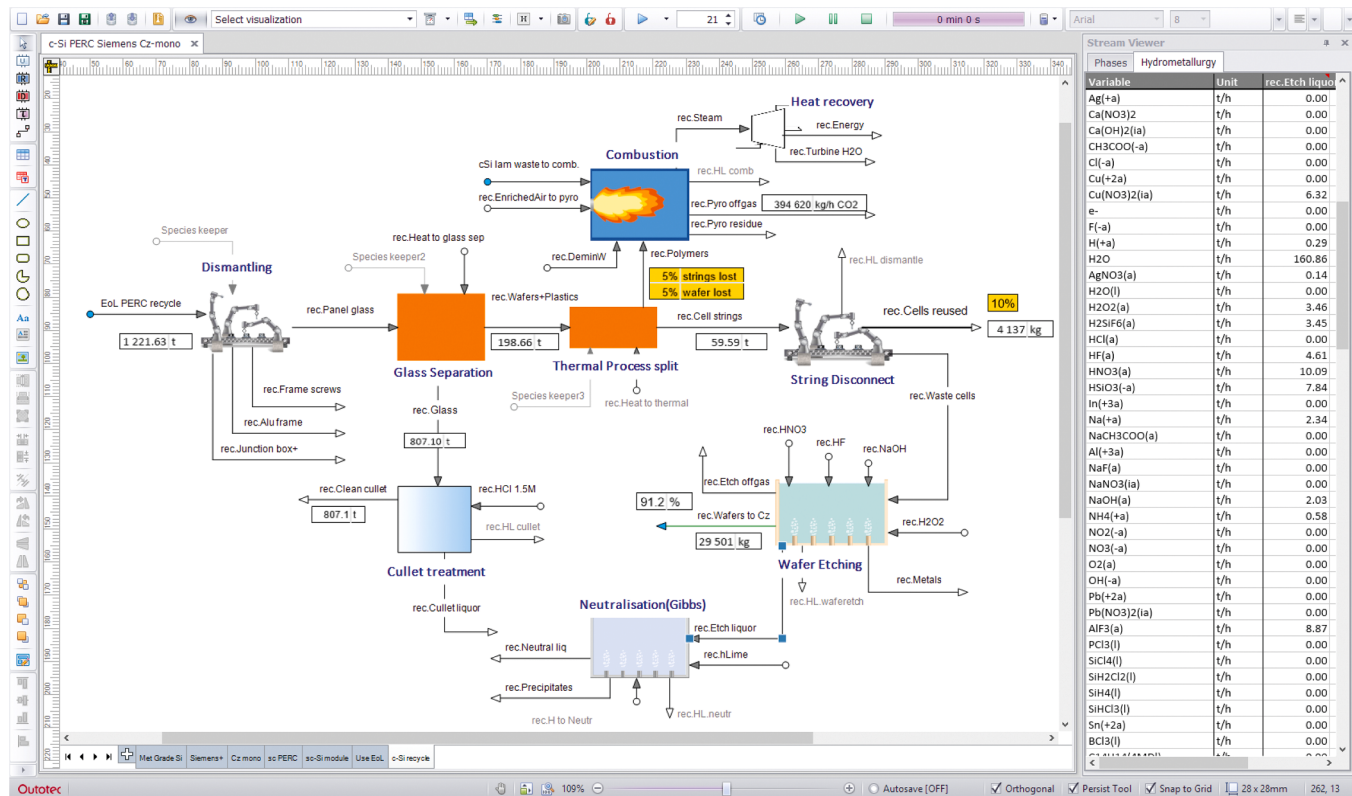


Fig. A2.7. Simulation flowsheet for PV module EOL recycling (wafer etching liquor composition shown on the right).

¹ FRELP – Full Recovery End of Life Photovoltaic process, developed by SASIL ([https://frelp.info](https://freelp.info))

² ASU – Arizona State University ([Huang et al. 2017](#))

chemistry for metal extraction, which allows for more control over the process (Huang et al., 2017). The authors report recoveries of 74% and 83% at purities of more than 99% for Ag and Cu, respectively, and the removal of more than 99% of Pb²⁺ from solution. Furthermore, 85–90% of Si can be recovered as SG-Si. In a previous study (Bartie et al., 2020), we modelled a PV-dedicated recycling process for CdTe PV modules based on First Solar's processing route, which also consists of delamination, glass recovery, and metal recovery steps (Wade, 2014).

Complete combustion of the polymers (EVA, PET, PVF, and PVB) and a 5% loss of cells and strings are assumed to occur in this step. Polymer combustion is used to estimate direct CO₂ generation (i.e. Scope 1 emission) according to the following chemical reactions:



The assumption of complete combustion is conservative in terms of GHG emissions as it likely overestimates the quantity of CO₂ generated. Hydrogen fluoride (HF) formed during the combustion of PVF is absorbed in a scrubber for neutralisation. Heat generated during this combustion process is partially recovered to generate electricity.

From string dismantling, it is assumed that 10% of cells are recovered intact for direct reuse. The remaining cells strings proceed to the leaching and etching steps to recover metals and wafer Si for reuse. Firstly, leaching in HNO₃ dissolves only Ag, Pb, and Cu, and precipitates Sn as SnO₂ i.e. the Sn/Pb solder, Sn-coated Cu ribbons, and the Ag contacts. Huang et al. (2017) then recover Ag, Cu in sequential electrowinning (EW) steps with Pb precipitating as hydrated PbO₂ during Cu recovery (see also Mecucci and Scott, 2002), while the SnO₂ precipitate is recovered by filtration. The EW steps are not included in the simulation, but their reported metal recoveries are taken into account in overall material efficiency calculations. Next, HF is used to dissolve only the SiN_x and Al-containing layers from the cells. The emitter and BSF are etched away in NaOH, a process that needs careful control as it is not self limiting (Huang et al., 2017). The leaching steps are simulated using the following reactions:



A stream of clean wafers is produced and recycled to the Cz crystallisation process as SG-Si feedstock. The remaining acidic liquor is neutralised with hydrated lime (Ca(OH)₂) to form calcium fluoride (CaF₂). Gibbs free energy minimization is used in this unit operation to estimate the compositions of the remaining neutral liquor and precipitates.

References

- Abadías Llamas, A., Valero Delgado, A., Valero Capilla, A., Torres Cuadra, C., Hultgren, M., Peltomäki, M., Roine, A., Stelter, M., Reuter, M.A., 2019. Simulation-based exergy, thermo-economic and environmental footprint analysis of primary copper production. Miner. Eng. 131, 51–65. <https://doi.org/10.1016/j.mine.2018.11.007>.
- Allen, T.G., Bullock, J., Yang, X., Javey, A., Wolf, S.de, 2019. Passivating contacts for crystalline silicon solar cells. Nature Energy 4 (11), 914–928. <https://doi.org/10.1038/s41560-019-0463-6>.
- Amini, S.H., Remmerswaal, J.A.M., Castro, M.B., Reuter, M.A., 2007. Quantifying the quality loss and resource efficiency of recycling by means of exergy analysis. J. Clean. Prod. 15 (10), 907–913. <https://doi.org/10.1016/j.jclepro.2006.01.010>.
- Ardente, F., Latunussa, C.E.L., Blengini, G.A., 2019. Resource efficient recovery of critical and precious metals from waste silicon PV panel recycling. Waste Manag. 91, 156–167. <https://doi.org/10.1016/j.wasman.2019.04.059>.
- Bartie, N.J., Abadías Llamas, A., Heibeck, M., Fröhling, M., Volkova, O., Reuter, M.A., 2020. The simulation-based analysis of the resource efficiency of the circular economy – the enabling role of metallurgical infrastructure. Mineral Process. Extract. Metall. 129 (2), 229–249. <https://doi.org/10.1080/25726641.2019.1685243>.
- Blakers, A., 2019. Development of the PERC Solar Cell. IEEE J. Photovoltaic. 9 (3), 629–635. <https://doi.org/10.1109/JPHOTOV.2019.2899460>.
- Blieske, U., Stollwerck, G., 2013. Glass and other encapsulation materials. In: Semiconductors and Semimetals. Advances in Photovoltaics: Part 2 (Vol. 89, pp. 199–258). Elsevier. <https://doi.org/10.1016/B978-0-12-381343-5.00004-5>.
- Bye, G., Ceccaroli, B., 2014. Solar grade silicon: technology status and industrial trends. Solar Energy Mater. Solar Cells 130, 634–646. <https://doi.org/10.1016/j.solmat.2014.06.019>.
- Casalino, G., Facchini, F., Mortello, M., Mummolo, G., 2016. IFAC-PapersOnLine. In: IFAC-PapersOnLine, 49, pp. 378–383. <https://doi.org/10.1016/j.ifacol.2016.07.634>.
- Ceccaroli, B., Lohne, O., 2011. Solar Grade Silicon Feedstock (2011). In: Luque, A., Hegedus, S. (Eds.), Handbook of Photovoltaic Science and Engineering, 2nd ed. Wiley; Chichester: John Wiley.
- Chandrasekaran, S.R., Hopke, P.K., Rector, L., Allen, G., Lin, L., 2012. Chemical composition of wood chips and wood pellets. Energy & Fuels 26 (8), 4932–4937. <https://doi.org/10.1021/ef300884k>.
- Chigondo, F., 2018. From metallurgical-grade to solar-grade silicon: an overview. Silicon 10 (3), 789–798. <https://doi.org/10.1007/s12633-016-9532-7>.
- Ciftja, A., Engh, T.A., Tangstad, M., 2008. Refining and Recycling of Silicon: A Review. Norwegian University of Science and Technology, Faculty of Natural Science and Technology, Department of Materials Science and Engineering. Retrieved from. <http://hdl.handle.net/11250/244462>.
- Deng, R., Chang, N.L., Ouyang, Z., Chong, C.M., 2019. A techno-economic review of silicon photovoltaic module recycling. Renew. Sustain. Energy Rev. 109, 532–550. <https://doi.org/10.1016/j.rser.2019.04.020>.
- De Wild-Scholten, M.J., 2013. Energy payback time and carbon footprint of commercial photovoltaic systems. Solar Energy Mater. Solar Cells 119, 296–305. <https://doi.org/10.1016/j.solmat.2013.08.037>.
- Dingemans, G., van de Sanden, M.C.M., Kessels, W.M.M., 2010. Influence of the deposition temperature on the c-Si surface passivation by Al₂O₃ films synthesized by ALD and PECVD. Electrochem. Solid-State Lett. 13 (3), H76. <https://doi.org/10.1149/1.3276040>.
- Dincer, I., Cengel, Y.A., 2001. Energy, entropy and exergy concepts and their roles in thermal engineering. Entropy, 3, 116–149.
- Diwekar, U.M., Small, M., 2002. Process analysis approach to industrial ecology (2002). In: Ayres, R., Ayres, L. (Eds.), A Handbook of Industrial Ecology. Edward Elgar Publishing, pp. 114–137.

- Dold, P., 2015. Silicon crystallization technologies (2012). In: Willeke, G., Weber, E.R. (Eds.), *Advances in Photovoltaics. Semiconductors and Semimetals*. Elsevier, p. 39, 0080-8784: volume 92, Part 4.
- Duflou, J.R., Peeters, J.R., Altamirano, D., Bracquene, E., Dewulf, W., 2018. Demanufacturing photovoltaic panels: comparison of end-of-life treatment strategies for improved resource recovery. *CIRP Annals* 67 (1), 29–32. <https://doi.org/10.1016/j.cirp.2018.04.053>.
- European Union (EU) (2017a). Communication from the commission to the European parliament, the council, the european economic and social committee and the committee of the regions on the 2017 list of critical raw materials for the EU. Retrieved from <https://eur-lex.europa.eu/legal-content/EN/TXT/?uri=CELEX:52017DC0490>.
- European Union (EU) (2017b). Study on the review of the list of Critical Raw Materials - Critical Raw Materials Factsheets. Retrieved from http://publications.europa.eu/resource/cellar/7345e3e8-98fc-11e7-b92d-01aa75ed71a1.0001.01/DOC_1, DOI: 10.2873/398823.
- Ekvall, T., Finnveden, G., 2001. Allocation in ISO 14041—a critical review. *J. Clean. Prod.* 9 (3), 197–208. [https://doi.org/10.1016/s0959-6526\(00\)00052-4](https://doi.org/10.1016/s0959-6526(00)00052-4).
- European Commission (2018). Commission staff working document - report on critical raw materials and the circular economy. SWD(2018) 36 final.
- EnergySage (2020). Average solar panel size and weight: energySage. <https://news.energysage.com/average-solar-panel-size-weight/>.
- Fraunhofer I.S.E. (2020). Recent facts about photovoltaics in Germany [PDF file]. Retrieved from <https://www.ise.fraunhofer.de/en/publications/studies/recent-fact-s-about-pv-in-germany.html> (accessed 9 September 2020).
- Frischknecht, R., Itten, R., Sinha, P., de Wild-Scholten, M., Zhang, J., Fthenakis, V., Kim, H.C., Raugei, M., Stucki, M., 2015. Life cycle inventories and life cycle assessment of photovoltaic systems. *Int. Energy Agency (IEA) PVPS Task 12. Report T12-04:2015*.
- European Union, 2012. Directive 2012/19/EU of the european parliament and of the council of 4 July 2012 on waste electrical and electronic equipment (WEEE) (recast (Text with EEA relevance)). *Official J. Eur. Union L197/38*.
- Frischknecht, R., Heath, G., Raugei, M., Sinha, P., de Wild-Scholten, M., Fthenakis, V., Kim, H.C., Alsema, E., Held, M., 2016. Methodology guidelines on life cycle assessment of photovoltaic electricity. 3rd edition. IEA PVPS Task 12. International Energy Agency Photovoltaic Power Systems Programme. Report IEA-PVPS T12-06: 2016, ISBN 978-3-906042-38-1.
- Frischknecht, R., Stoltz, P., Krebs, L., de Wild-Scholten, M., Sinha, P., Fthenakis, V., Kim, H.C., Raugei, M., Stucki, M., 2020. Life cycle inventories and life cycle assessment of photovoltaic systems. *Int. Energy Agency (IEA) PVPS Task 12. Report T12-19:2020*, ISBN 978-3-907281-14-7.
- Fröhling, M., Schwaderer, F., Bartusch, H., Schultmann, F., 2013. A material flow-based approach to enhance resource efficiency in production and recycling networks. *J. Ind. Ecol.* 17 (1), 5–19. <https://doi.org/10.1111/j.1530-9290.2012.00502.x>.
- Gong, J., Darling, S.B., You, F., 2015. Perovskite photovoltaics: life-cycle assessment of energy and environmental impacts. *Energy Environ Sci* 8 (7), 1953–1968. <https://doi.org/10.1039/c5ee00615e>.
- Greenhouse Gas Protocol (2016). Global warming potential values. Retrieved from https://www.ghgprotocol.org/sites/default/files/ghgp/Global-Warming-Potential-Values%20%28Feb%2016%202016%29_1.pdf.
- Greenhouse Gas Protocol (2011). Product life cycle accounting and reporting standard. Retrieved from https://ghgprotocol.org/sites/default/files/standards/Product-Life-Cycle-Accounting-Reporting-Standard_041613.pdf.
- GTT-Technologies (2020). FactSage version 7.2 [Computer software]. Retrieved from <https://gtt-technologies.de/software/factsage/>.
- Haegel, N.M., Atwater, H., Barnes, T., Breyer, C., Burrell, A., Chiang, Y.-M., Wolf, S., de, Dimmier, B., Feldman, D., Glunz, S., Goldschmidt, J.C., Hochschild, D., Inzunza, R., Kaizuka, I., Kroposki, B., Kurtz, S., Leu, S., Margolis, R., Matsubara, K., Bett, A.W., 2019. Terawatt-scale photovoltaics: transform global energy. *Science* 364 (6443), 836–838. <https://doi.org/10.1126/science.aaw1845>.
- Hahn, G., Joos, S., 2014. State-of-the-art industrial crystalline silicon solar cells. In: *Semiconductors and Semimetals. Advances in Photovoltaics: Part 3* (Vol. 90, pp. 1–72). Elsevier. <https://doi.org/10.1016/B978-0-12-388417-6.00005-2>.
- Halvorsen, T., Moen, M., Mork, K., Grosset-Bourbange, D., Rivat, P., Hajjaji, H., Brizé, V., & Coutier, F. (2017). CabriSS: recycling of Si-Kerf from PV. Advance online publication. 10.4229/EUPSEC20172017-5EO.1.5 (4 pages /33rd European Photovoltaic Solar Energy Conference and Exhibition; 1524–1527 / 33rd European Photovoltaic Solar Energy Conference and Exhibition; 1524–1527).
- Heath, G.A., Silverman, T.J., Kempe, M., Deceglie, M., Ravikumar, D., Remo, T., Cui, H., Sinha, P., Libby, C., Shaw, S., Komoto, K., Wambach, K., Butler, E., Barnes, T., Wade, A., 2020. Research and development priorities for silicon photovoltaic module recycling to support a circular economy. *Nature Energy* 5 (7), 502–510. <https://doi.org/10.1038/s41560-020-0645-2>.
- Hirtz, W., Huber, W., Kolb, G., 1992. Berichte Des Forschungszentrums Jülich 1993: Angewandte Systemanalyse Nr. 67: Umweltvorsorgeprüfung bei Forschungsvorhaben, Am Beispiel Von Photovoltaik, Band 6. Praktische Durchführung. Nr. 2757, ISSN 0366-0885.
- Hofmann, M., Kohn, N., Schwarz, F., Nöller, S., Kastl, S., Beckmann, R., Ferré, R., Pernau, T., Trogus, D., Kühnhold, S., Saint-Cast, P., & Rentsch, J. (2013). High-Power-Plasma PECVD of SiNx and Al2O3 for industrial solar cell manufacturing. Advance online publication. 10.4229/28THEUPSEC2013-2BV.1.45 (4 pages /28th European Photovoltaic Solar Energy Conference and Exhibition; 1184–1187 / 28th European Photovoltaic Solar Energy Conference and Exhibition; 1184–1187).
- Huang, W.-H., Shin, W.J., Wang, L., Sun, W.-C., Tao, M., 2017. Strategy and technology to recycle wafer-silicon solar modules. *Solar Energy* 144, 22–31. <https://doi.org/10.1016/j.solener.2017.01.001>.
- IEA PVPS (2019). Trends in Photovoltaic Applications 2019. International Renewable Energy Agency and International Energy Agency Photovoltaic Power Systems, Report IEA PVPS T1-36: 2019. Retrieved from <https://iea-pvps.org/wp-content/uploads/2020/02/5319-iea-pvps-report-2019-08-1r.pdf>.
- IEA (2020a). Clean energy technology innovation and the vital role of governments. Retrieved from <https://www.iea.org/reports/clean-energy-innovation/clean-energy-technology-innovation-and-the-vital-role-of-governments>.
- IEA (2020b). Countries and regions. Retrieved from <https://www.iea.org/countries> (accessed 7 October 2020).
- Jakobsson, L.K., Tangstad, M., 2014. Distribution of Boron Between Silicon and CaO-MgO-Al2O3-SiO2 Slags. *Metallurgical and Materials Transactions B* 45 (5), 1644–1655. <https://doi.org/10.1007/s11663-014-0088-x>.
- Jiang, L., Fieselman, B.F., Chen, L., Mixon, D., 2017. Fluidized bed process with silane. In: Yang, D. (Ed.), *Handbook of Photovoltaic Silicon* (Vol. 29, pp. 1–40). Springer Berlin Heidelberg. <https://doi.org/10.1007/978-3-662-52735-1-5-1>.
- Jiao, Y., Salce, A., Ben, W., Jiang, F., Ji, X., Morey, E., Lynch, D., 2011. Siemens and Siemens-like Processes for Producing Photovoltaics: energy Payback Time and Lifetime Carbon Emissions. *Journal of Metals* 63 (1).
- Jungbluth, N., Stucki, M., Frischknecht, R., Buesser, S., et al., 2010. Photovoltaics. In: Dones, R., et al. (Eds.), *Sachbilanzen Von Energiesystemen: Grundlagen für den ökologischen Vergleich Von Energiesystemen und Den Einbezug von Energiesystemen in Ökobilanzen für die Schweiz*. EcoInvent Report No. 6-XII. ESU-services Ltd, Uster, CH, 2010.
- Kubat, M., 2017. An Introduction to Machine Learning. Springer International Publishing. <https://doi.org/10.1007/978-3-319-63913-0>.
- Klatt, K.-U., Marquardt, W., 2009. Perspectives for process systems engineering—Personal views from academia and industry. *Comput. Chem. Eng.* 33 (3), 536–550. <https://doi.org/10.1016/j.compchemeng.2008.09.002>.
- Lan, C., Hsieh, C., Hsu, W., 2009. Czochralski Silicon Crystal Growth for Photovoltaic Applications (2009). In: Nakajima, K., Usami, N. (Eds.), *Crystal Growth of Si for Solar cells. Advances in Materials Research*, 1435–1889: Vol. 14. Springer. <http://www.springer.com/gb/BLDSS>.
- Latunussa, C.E.L., Ardenté, F., Blengini, G.A., Mancini, L., 2016. Life Cycle Assessment of an innovative recycling process for crystalline silicon photovoltaic panels. *Solar Energy Mater. Solar Cells* 156, 101–111. <https://doi.org/10.1016/j.solmat.2016.03.020>.
- Li, H., Kim, K., Hallam, B., Hoex, B., Wenham, S., Abbott, M., 2017. POCl3 diffusion for industrial Si solar cell emitter formation. *Front. Energy* 11 (1), 42–51. <https://doi.org/10.1007/s11708-016-0433-7>.
- Louwen, A., van Sark, W.G.J.H.M., Schropp, R.E.I., Turkenburg, W.C., Faaij, A.P.C., 2015. Life-cycle greenhouse gas emissions and energy payback time of current and prospective silicon heterojunction solar cell designs. *Progr. Photovoltaics* 23 (10), 1406–1428. <https://doi.org/10.1002/pip.2540>.
- Lozano, M.A., Valero, A., 1993. Theory of the exerggetic cost. *Energy* 18 (9), 939–960. [https://doi.org/10.1016/0360-5442\(93\)90006-Y](https://doi.org/10.1016/0360-5442(93)90006-Y).
- Mandal, N.C., Acharya, S., Biswas, S., Panda, T., Sadhukhan, S., Sharma, J.R., Bose, S., Das, G., Kole, A., Nandi, A., Maity, S., Chaudhuri, P., Saha, H., Guha, S., 2020. Evolution of PERC from Al-BSF: optimization based on root cause analysis. *Appl. Phys. A* 126 (7), 1163. <https://doi.org/10.1007/s00339-020-03747-4>.
- MathWorks (2020). MATLAB version R2019b [Computer software]. Retrieved from <http://www.mathworks.com/products/matlab.html>.
- MathWorks (2020b). trainbr – Bayesian regularization propagation. Retrieved from <http://www.mathworks.com/help/deeplearning/ref/trainbr.html?tid=srchtitle>.
- MathWorks (2020c). plotperform – Plot network performance. Retrieved from <http://www.mathworks.com/help/deeplearning/ref/plotperform.html>.
- Mecucci, A., Scott, K., 2002. Leaching and electrochemical recovery of copper, lead and tin from scrap printed circuit boards. *J. Chem. Technol. Biotechnol.* 77 (4), 449–457. <https://doi.org/10.1002/jctb.575>.
- Michas, S., Stavrakas, V., Spyridaki, N.-A., Flamos, A., 2019. Identifying research priorities for the further development and deployment of solar photovoltaics. *Int. J. Sustain. Energy* 38 (3), 276–296. <https://doi.org/10.1080/14786451.2018.1495207>.
- Miki, T., Morita, K., Sano, N., 1996. Thermodynamics of phosphorus in molten silicon. *Metallurgic. Mater. Trans. B* 27 (6), 937–941. <https://doi.org/10.1007/s11663-996-0007-x>.
- Muteri, V., Cellura, M., Curto, D., Franzitta, V., Longo, S., Mistretta, M., Parisi, M.L., 2020. Review on life cycle assessment of solar photovoltaic panels. *Energies* 13 (1), 252. <https://doi.org/10.3390/en13010252>.
- NREL (2020). Q4 2019 /Q1 2020 solar industry update. NREL/PR-6A20-77010, retrieved from <https://www.nrel.gov/docs/fy20osti/77010.pdf>.
- Outotec (2020). HSC chemistry version 10.0.0.8 [Computer software]. Retrieved from <https://www.outotec.com/products-and-services/technologies/digital-solutions/hsc-chemistry/>.
- Øvreliid, E., Pizzini, S., 2017. Chapter 2 The MG silicon route. In: Ceccaroli, B., Øvreliid, E., Pizzini, S. (Eds.), *Solar Silicon Processes: Technologies, Challenges, and Opportunities*. CRC Press, pp. 49–82. <https://doi.org/10.1201/9781315369075-3>.
- PCC (2017) PCC Bakki Silicon – The technology. Retrieved from <http://www.pcc.is/the-plant-technology/>.
- Peguirón, J., Mueller, R., Zanetti, J., Habegger, S., Burri, M. & Monti di Sopra, F. (2014). Reducing wire wear by mechanical optimization of equipment in diamond-wire wafering. Retrieved from meyerburger.com.
- PVTECH (2020a). Trina Solar betting on largest wafer size and third cut cells for 500W-plus modules. Retrieved from <https://www.pv-tech.org/news/trina-solar-betting-on-largest-wafer-size-and-third-cut-cells-for-500w-plus>.

- PVTECH (2020b). RENA secures 15GW M12 wafer and solar cell cleaning equipment order. Retrieved from <https://www.pv-tech.org/news/rena-secures-15gw-m12-wafer-and-solar-cell-cleaning-equipment-order>.
- Ramírez-Márquez, C., Otero, M.V., Vázquez-Castillo, J.A., Martín, M., Segovia-Hernández, J.G., 2018. Process design and intensification for the production of solar grade silicon. *J. Clean. Prod.* 170, 1579–1593. <https://doi.org/10.1016/j.jclepro.2017.09.126>.
- REC (2019). REC Silicon - Annual Report 2019. Retrieved from <https://www.globenewswire.com/news-release/2020/03/24/2005801/0/en/REC-Silicon-Annual-Report-2019.html>.
- Reuter, M.A., 1998. The simulation of industrial ecosystems. *Miner. Eng.* 11 (10), 891–918. [https://doi.org/10.1016/S0892-6875\(98\)00078-8](https://doi.org/10.1016/S0892-6875(98)00078-8).
- Reuter, M.A., 2016. Digitalizing the circular economy. *Metallurgic. Mater. Trans. B* 47 (6), 3194–3220. <https://doi.org/10.1007/s11663-016-0735-5>.
- Reuter, M.A., van Schaik, A., Gutzmer, J., Bartie, N., Abadías-Llamas, A., 2019. Challenges of the circular economy: a material, metallurgical, and product design perspective. *Annu. Rev. Mater. Res.* 49 (1), 253–274. <https://doi.org/10.1146/annurev-matsci-070218-010057>.
- Reuter, M.A., Walt, T.J., Deventer, J.S.J., 1992. Modeling of metal-slag equilibrium processes using neural nets. *Metallurgic. Mater. Trans. B* 23 (5), 643–650. <https://doi.org/10.1007/BF02649724>.
- Rodriguez, H., Guerrero, I., Koch, W., Endrös, A.L., Franke, D., Häfler, C., Kalejs, J.P., Möller, H.J., 2011. Bulk crystal growth and wafering for PV (2011). In: Luque, A., Hegedus, S. (Eds.), *Handbook of Photovoltaic Science and Engineering*, 2nd ed. Wiley: Chichester. John Wiley.
- ROSI Solar, 2020. ROSI is awarded first “Green Deal” funding. Retrieved from <https://www.rosi-solar.com/rosi-is-awarded-first-green-deal-funding/>.
- Safarian, J., Tramell, G., Tangstad, M., 2012. Processes for upgrading metallurgical grade silicon to solar grade silicon. *Energy Procedia* 20, 88–97. <https://doi.org/10.1016/j.egypro.2012.03.011>.
- Seigneur, H., Mohajeri, N., Brooker, R.P., Davis, K.O., Schneller, E.J., Dhore, N.G., Rodgers, M.P., Wohlgemuth, J., Shiradkar, N.S., Scardera, G., Rudack, A.C., Schoenfeld, W.V., 2016. Manufacturing metrology for c-Si photovoltaic module reliability and durability, Part I: feedstock, crystallization and wafering. *Renew. Sustain. Energy Rev.* 59, 84–106. <https://doi.org/10.1016/j.rser.2015.12.343>.
- Sica, D., Malandrino, O., Supino, S., Testa, M., Lucchetti, M.C., 2018. Management of end-of-life photovoltaic panels as a step towards a circular economy. *Renew. Sustain. Energy Rev.* 82, 2934–2945. <https://doi.org/10.1016/j.rser.2017.10.039>.
- Stoltz, P., Frischknecht, R., Wambach, K., Sinha, P., Heath, G., 2017. Life cycle assessment of current photovoltaic module recycling. IEA PVPS Task 12. International Energy Agency Power Systems Programme. Report IEA-PVPS T12-13:2018.
- thinkstep (2018). GaBi Software-System and Database for Life Cycle Engineering, version 8.7, database schema 8007 [Computer software]. Retrieved from <http://www.gabi-software.com/deutsch/index/>.
- Tsanakas, J.A., Heide, A., Radavičius, T., Denafas, J., Lemaire, E., Wang, K., Poortmans, J., Voroshazi, E., 2020. Towards a circular supply chain for PV modules: review of today's challenges in PV recycling, refurbishment and re-certification. *Progr. Photovoltaics* 28 (6), 454–464. <https://doi.org/10.1002/pip.3193>.
- VDMA (2020). International Roadmap for Photovoltaic (ITRPV), 11th edition, April 2020. Retrieved from <https://itrpv.vdma.org/en/>.
- UNEP, 2013. United Nations Environment Programme. International Resource Panel. Metal recycling. Opportunities, limits, infrastructure. International Resource Panel, issuing body, Nairobi.
- Verhoef, E.V., Dijkema, G.P.J., Reuter, M.A., 2004. Process Knowledge, System Dynamics, and Metal Ecology. *Journal of Industrial Ecology* 8 (1–2), 23–43. <https://doi.org/10.1162/1088198041269382>.
- Wade, A., 2014. Evolution of first Solar's module recycling technology. Workshop on PV Life Cycle Management and Recycling at the 29th EU-PVSEC. Amsterdam, the Netherlands. September 2014.
- Wade, A., Sinha, P., Drozdík, K., Brutsch, E., 2017. Beyond waste – the fate of end-of-life photovoltaic panels from large scale PV installations in the EU - the socio-economic benefits of high value recycling compared to re-use. *Proc. 33rd European Photovoltaic Solar Energy Conference. WIP Wirtschaft und Infrastruktur GmbH & Co Planungs-KG, Amsterdam*, pp. 1507–1514, 2017.
- Wernet, G., Bauer, C., Steubing, B., Reinhard, J., Moreno-Ruiz, E., Weidema, B., 2016. The ecoinvent database version 3 (part I): overview and methodology. *Int. J. Life Cycle Assess.* 21 (9), 1218–1230. <https://doi.org/10.1007/s11367-016-1087-8>.
- Werner, S., Lohmüller, E., Saint-Cast, P., Greulich, J.M., Weber, J., Schmidt, S., Moldovan, A., Brand, A.A., Dannenberg, T., Mack, S., Wasmer, S., Demant, M., Linse, M., Ackermann, R., Wolf, A., Preu, R., 2017. Key aspects for fabrication of P-type Cz-Si perc solar cells exceeding 22% conversion efficiency. Presented At the 33rd European PV Solar Energy Conference and Exhibition, 24–29 September 2017. Amsterdam, The Netherlands.
- Wirth, H., 2013. Crystalline Silicon PV module technology. In: Semiconductors and Semimetals. *Advances in Photovoltaics: Part 2* (Vol. 89, pp. 135–197). Elsevier. <https://doi.org/10.1016/B978-0-12-381343-5.00003-3>.
- Edited by Xakalashe, Buhle, Tangstad, Merete, 2011. Silicon processing: from quartz to crystalline silicon solar cells. In: Jones, R.T., den Hoed, P. (Eds.), *Southern African Pyrometallurgy 2011*. Southern African Institute of Mining and Metallurgy, Johannesburg. Edited by 6–9 March 2011.
- Yan, D., 2017. Siemens Process. In: Yang, D. (Ed.), *Handbook of Photovoltaic Silicon* (Vol. 42, pp. 1–31). Springer Berlin Heidelberg. https://doi.org/10.1007/978-3-662-52735-1_4-2.
- Yifan, Z., Sihai, C., Edmond, S., Bosseboeuf, A., 2013. Deep wet etching in hydrofluoric acid, Nitric Acid, and Acetic Acid of cavities in a silicon wafer. *Jpn. J. Appl. Phys.* 52 (7R), 76503. <https://doi.org/10.7567/JJAP.52.076503>.
- Zulehner, W., Neuer, B., Rau, G., 2000. Silicon. In: Ullmann's Encyclopedia of Industrial Chemistry. Wiley-VCH Verlag GmbH & Co. KGaA. https://doi.org/10.1002/14356007.a23_721.